Spatially and temporally targeted neuromodulation by transcranial electrical stimulation

Doctoral Thesis

Mihály Vöröslakos

Szeged, 2019

Spatially and temporally targeted neuromodulation by transcranial electrical stimulation

Doctoral Thesis

Mihály Vöröslakos

Department of Physiology
Faculty of Medicine, University of Szeged

Szeged, 2019

List of publications

Publications related to the subject of the thesis

I. *Mihály Vöröslakos*, Yuichi Takeuchi, Kitti Brinyiczki, Tamás Zombori, Azahara Oliva, Antonio Fernández-Ruiz, Gábor Kozák, Zsigmond Tamás Kincses, Béla Iványi, György Buzsáki, Antal Berényi (2018)
Direct effects of transcranial electric stimulation on brain circuits in rats and humans
Nature Communications
DOI: 10.1038/s41467-018-02928-3

II. Anli Liu, *Mihály Vöröslakos*, Greg Kronberg, Simon Henin, Matthew R. Krause, Yu Huang, Alexander Opitz, Ashesh Mehta, Christopher C. Pack, Bart Krekelberg, Antal Berényi, Lucas C. Parra, Lucia Melloni, Orrin Devinsky, György Buzsáki (2018)
Immediate neurophysiological effects of transcranial electrical stimulation
Nature Communications
DOI: 10.1038/s41467-018-07233-7

Other publications

I. Komal Kampasi, Daniel F. English, John Seymour, Eran Stark, Sam McKenzie, *Mihály Vöröslakos*, György Buzsáki, Kensall D. Wise, Euisik Yoon (2018)
Dual color optogenetic control of neural populations using low-noise, multishank optoelectrodes
Microsystems & Nanoengineering
DOI: 10.1038/s41378-018-0009-2

II. Adam E. Mendrela, Sung-Yun Park, *Mihály Vöröslakos*, Michael P. Flynn, Euisik Yoon (2018)
A battery-powered opto-electrophysiology neural interface with artifact preventing optical pulse shaping
IEEE Symposium on VLSI Circuits 2018
DOI: 10.1109/VLSIC.2018.8502353

III. Kyounghwan Na, Zachariah J Sperry, Jiaao Lu, *Mihály Vöröslakos*, Saman S Parizi, Tim M Bruns, Euisik Yoon, John P Seymour (2018)
Novel diamond shuttle to deliver flexible bioelectronics with reduced tissue compression
bioRxiv
DOI: 10.1101/435800

IV. Kanghwan Kim, *Mihály Vöröslakos*, John P. Seymour, Kensall D. Wise, György Buzsáki, Euisik Yoon (2019)
Artifact-free, high-temporal-resolution in vivo opto-electrophysiology with microLED optoelectrodes
bioRxiv
DOI: 10.1101/622670

“Research is to see what everybody has seen and think what nobody has thought.”

Albert Szent-Györgyi
/1957/

Table of contents

Introduction 1
Fundamentals of electrical stimulation of neural tissue 2
Electric fields in biological materials 2
Effects of the tissues of the head on the intracerebral current distributions 3
The effect of stimulation polarity 3
Stimulation intensity 6
Electrode montages, electrode sizes 7
Stimulus waveform (tDCS and tACS) 8
Safety 9
Instantaneous effects of electric field 10
Immediate neuronal effects of TES 11
Aims of the research 15
Results 16
Comparison of sub- and transcutaneous electrical stimulation in rats 16
Measuring current spread through scalp, skull and brain in human cadavers 19
Affecting human brain network activity by ISP stimulation 22
Focused TES effect by ISP stimulation 27
Discussion 30
TES-induced physiological effects 30
Current flow through the scalp, skull and brain 31
ISP: injecting high current intensities and targeting brain regions 32
Materials and methods 35
Experiments on rats 35
Comparison of transcutaneous and subcutaneous TES in vivo 35
Measuring the effect of postmortem age 37
Measurements on human cadavers 37
Recording tACS-induced intracerebral electric fields 37
Measuring the shunting effect of the skin and skull in human cadavers 39
Registering the anthropometric data of the cadavers 40
ISP stimulation on human subjects 41
EEG recording during ISP stimulation 41
ISP stimulation induced artefact removal 42
Frequency-amplitude and phase-amplitude analysis of EEG 43
ISP stimulation in rats 44
Modeling of ISP stimulation induced electric fields 44
In vivo, extracellular recordings during ISP stimulation 44
Comparing the effect of DC and ISP stimulation 45
Acknowledgments 47
References 48

Introduction

Electrical stimulation whether invasive or noninvasive is one of the oldest perturbation approaches in neuroscience. Ancient and medieval attempts used electric fishes (T. torpedo) to treat pain; although the basic physical principles of electricity, and consequently the modern brain stimulation techniques were developed only later in the 19th and 20th centuries[1]. In the late 1930s electroconvulsive therapy (ECT) was introduced as the first scientifically established neurostimulation application to treat several neuropsychological disorders in humans[2]. In parallel, research has also been focused on the delivery of a more localized electrical stimulation. Two techniques emerged, an invasive one called deep brain stimulation (DBS) and a noninvasive one called transcranial electrical stimulation (TES). Thanks to the continuous progress of stereotactic methods, numerous studies showed that high-frequency DBS was able to decrease tremor symptoms[3]. Since then, DBS has been approved as a treatment for numerous neuropsychological disorders, e.g.: Parkinson's disease, essential tremor, dystonia and obsessive–compulsive disorder[4]. DBS is also used in many scientific studies; however, due to its invasive nature its accessibility is limited and imposes a non-negligible risk of serious complications. That is one of the reasons why researchers' interest has grown exponentially in noninvasive brain stimulation (NIBS) methods like transcranial electrical and magnetic stimulation (TMS). Despite its relative simplicity, TES has not become a popular research tool until 2000 when Nitsche and Paulus showed that weak electrical current stimulation over the motor cortex was able to induce changes in brain excitability[5]. Since then, the following main methods of TES have been investigated: transcranial direct current stimulation (tDCS), transcranial alternating current stimulation (tACS) and transcranial random noise stimulation (tRNS). Its noninvasiveness allows widespread application to subjects; therefore, TES has been increasingly introduced as a clinical tool for the treatment of neuropsychiatric disorders (e.g.: major depression, migraine, tinnitus, addiction and schizophrenia[6]). Despite the initial promising empirical results of the clinical trials and growing number of publications (Figure 1), the exact mechanisms by which electrical stimulation can affect neural activity has remained unknown. In order to optimize the efficacy of neurostimulation therapies we need a better understanding on the basic neurophysiological, electrochemical and biophysical concepts of their effects.

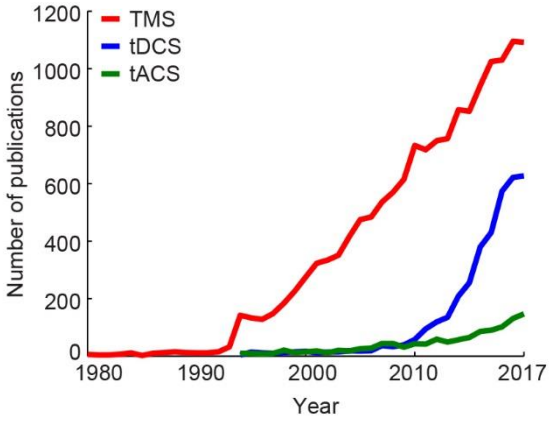

Figure 1 NIBS publication per year
Growing number of publications per year for TMS, tDCS and tACS (source: Web of Science; from 1980 to 2017)

Fundamentals of electrical stimulation of neural tissue

Electrical stimulation can induce graded changes in the extracellular potential level (V_e), thus, can create induced electric fields in the brain. Similarly, neuronal activity can also induce focal changes in V_e by sinking and emitting charged particles, and thus can also create 'endogenous' electric fields. Regardless of the origin, such fields by definition alter the transmembrane potential (V_m) of adjacent neurons and modulate the ongoing brain activity[7–9].

Electric fields in biological materials

At each point within the brain, a scalar electric potential can be measured relative to an arbitrary reference and expressed in Volts (V). The electric field $\vec{E}$ is the local change (gradient) of the voltage; $\vec{E}$ is a vector whose amplitude is measured in Volts per meter (V/m). All transmembrane currents from nearby neuronal processes contribute to generate $\vec{E}$[10]. When a current is applied to brain tissue (as in TES), it affects the polarization of cellular membranes, which in turn can alter neuronal excitability. The current that flows in the scalp, skull and brain during TES depends on 1) the conductivity of the different tissues of the head, 2) the applied current intensity (in mA) and 3) the stimulating electrode size and position.

It is important to understand how these parameters can affect the current spread and lead to modulation of neuronal elements far away from the stimulating electrodes.

Effects of the tissues of the head on the intracerebral current distributions

The frequencies used in electrical stimulation are in the range from DC to 5 kHz[11]. Below 5 kHz, the conductivity of body tissues is relatively constant, therefore, biological tissues are mostly resistive in this frequency range[12,13]. In this section, I am going to focus on the biophysics of the human head only.

The scalp is composed of multiple different tissues with variable physiological and electrical properties. TES studies adopted some simplification and divide the scalp into three different layers: skin, fat and muscle. Due to its heterogeneous nature, the local conductivity within the scalp can vary greatly. In general, the skin has high conductivity (0.5 S/m); however, the dry superficial layer is highly resistive (0.0001 S/m)[14]. In healthy adults with normal body mass index (BMI), there is around 2 mm of subcutaneous fat, which has low conductivity (0.04 S/m) and its effect on the overall conductivity of the scalp is minor. However, thick layer of subcutaneous fat (BMI > 35) can have a significant impact[15]. The conductivity of muscle depends on the direction of its fibers (longitudinal direction – 0.6 S/m; perpendicular direction – 0.1 S/m)[12,16]. Muscles near or under the stimulating electrodes can reduce the current reaching the brain due to shunting through those muscles[17].

The conductivity of the skull is also anisotropic because of its structure. The skull consists of a central spongious bone enclosed by two layers of compact bone. The former has 4 times higher conductivity than that of compact bone (0.08 S/m vs 0.02 S/m)[12,13]. In addition, the skull thickness is not uniform, it varies greatly in different parts of the calvarium (Table 1). Quite surprisingly, a recent modeling study did not find a clear linear relationship between the skull thickness and the induced electric field; however, the composition and thickness of the bone had an overall influence on the magnitude of the induced electric field[18].

Regarding the brain tissue, grey matter has high conductivity (0.4 S/m) and it is usually described as a homogeneous and isotropic medium[19]. However, white matter shows anisotropy; its longitudinal conductivity (1.1 S/m) is 11 times higher than its transverse one (0.1 S/m)[20]. Due to the inhomogeneity of brain tissue, TES induces a complex, 3-dimensional current flow in the central nervous system.

The effect of stimulation polarity

While closing the circuit for transcranial electrical stimulation there is at least one electrode that acts as an anode where current is entering the head and at least another one

acting as a cathode where current is leaving the head. The anode is at a positive potential level compared to the cathode. Animal studies in the 1960s showed that electrical stimulation can produce polarity-specific effects. They found that spontaneous and evoked cortical activity could be increased under the anode and decreased under the cathode[21–23]. Their results suggested that the increased neuronal activity under the anode is due to 'membrane depolarization' whereas the decreased excitability under the cathode is due to 'membrane hyperpolarization'.

Nitsche and Paulus (2000) found similar tendencies in the TMS elicited motor-evoked potentials of healthy volunteers. Based on their results, they concluded: 'anodal stimulation of the motor cortex enhanced excitability, whilst it was diminished by cathodal stimulation'[5]. Their work created the convention that anodal stimulation will lead to cortical excitation whereas cathodal stimulation will lead to cortical inhibition. Since then, TES community adopted these terms and many studies either focus on the anodal (stimulatory) or the cathodal (inhibitory) effect of stimulation which means that the targeted brain region where an effect was desired was closer either to the anode or to the cathode. However, one should keep in mind that there is always a concurrent anode and a cathode present in any TES system, therefore, the stimulating electrodes cannot be considered separately[24]. All current that enters through the anode must exit through the cathode[25]. The terminology is even more misleading because it assumes that the neuronal effect of TES is based on the 'somatic doctrine' only[26].

The 'somatic doctrine' assumes that TES induced current flow will lead to soma polarization, which in turn, will determine the neuronal response to TES. It completely ignores that neuronal activity depends on the integration of postsynaptic potentials in all neuronal compartments (dendrites, axon hillock, presynaptic terminal). In addition, it does not consider that TES will induce both de- and hyperpolarization of membrane compartments in any given brain region[27–29]. Unfortunately, the concept is still commonly used in clinical literature, despite the fact that modeling and animal studies suggest a more complex effect of TES.

First of all, neuronal morphology relative to the electric field vector directions determines the polarity of effect in the subsequent neuronal compartments. Anodal stimulation will lead to somatic depolarization and apical dendrite hyperpolarization in a layer V pyramidal cell, which dendrites point toward the cortical surface (Fig. 2a, b). However, the orientation of neurons relative to the cortical surface depends on the presence of gyri and sulci. Recent *in silico* and *in vitro* studies showed that TES induces currents in both

radial (parallel to the somatodendritic axis) and tangential (perpendicular to the somatodendritic axis) direction in the human grey matter (Fig. 2c) which can further complicate the clinical outcome of TES[26]. In addition, the curvature of the gyri can also modify the shape of the induced electric field in the cortex, regardless its anodal or cathodal nature[30].

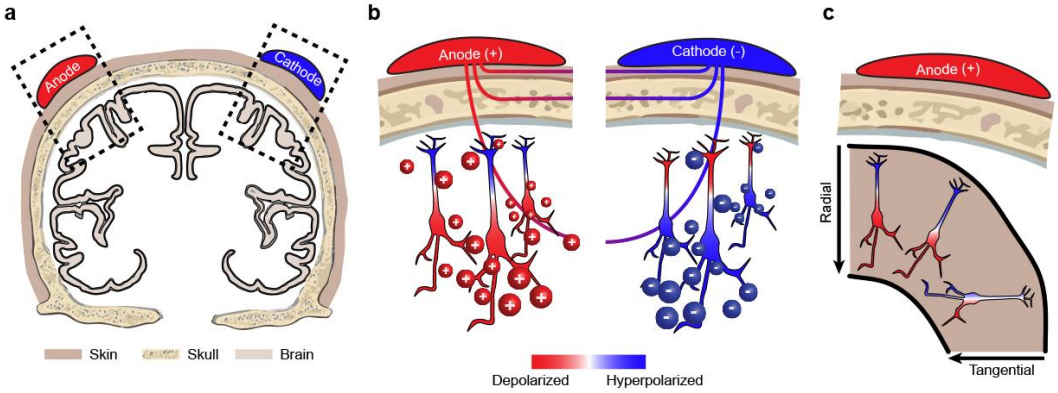

Figure 2 Neuronal polarization
a Schematic of transcranial electrical stimulation arrangement. Note that only the neocortical grey matter is displayed for simplicity. Red is anode blue is cathode. **b** Magnified view from **a**. Idealized layer V pyramidal neurons' membrane are polarized by TES (note the orientation is similar for each neuron, with the apical dendrite facing towards the stimulating electrode). Under the anode, there is inward current flow which will cause somatic depolarization and apical dendrite hyperpolarization. The opposite effect occurs under the cathode due to the outward current flow. **c** Effect of cortical folding on neuronal polarization. An idealized gyrus and three example neurons are shown. Note the different effect of TES due to the different orientations of the cell bodies. (Adopted from: The Stimulated Brain, 2014)[31]

In comparison, TES generates mostly radial currents in rodents due to the lack of cortical foldings, therefore, one should be careful when directly translating animal findings into human applications. Many clinical researchers are very much aware of the findings of animal studies, however, most of them are still designing their TES protocols to treat neuropsychiatric disorders based on the 'somatic doctrine' (e.g., anodal TES over left dorso-lateral prefrontal cortex is supposed to increase its excitability and is expected to treat depression[32]).

I do emphasize that the field requires more modeling, animal and clinical studies to better understand the mechanisms of action of TES because changes in neuronal activity due to anodal and/or cathodal stimulation are complicated and the empirical findings cannot be explained by the 'somatic doctrine' itself.

Stimulation intensity

To guarantee the reproducibility of intracerebral voltage gradients even with unstable electrode-skin interface resistance, all studies must use current controlled stimulation. By definition, intensity is the current intensity (in mA) of the steady-state (DC) or the peak (AC, n.b. the maximal instantaneous intensity, not the peak-to-peak intensity) current passing between the anode and cathode. Using multi-electrode techniques, the current intensity is the sum of the current at all anodes[33]. Electrode current density is another intensity related metrics frequently used in the literature. It is the applied current through a stimulation electrode divided by the electrode's surface area. The magnitude of TES induced electric fields and changes in neuronal activity scale linearly with current intensity[26,28,34].

In general, animal studies use wide range of current intensities (25 μA – 1 mA) and electrode current densities (5.12 ± 1.11 mA/cm^2; mean ± SEM) which can generate more than 5 V/m electric field in the brain. High intensities are used intentionally in order to detect neuronal response more reliably by reading out induced action potentials instead of the technically more challenging measurement of analog changes in E_m. To date, 0.2 V/m was found as the lowest electric field that was capable of altering neuronal activity *in vitro*, however the authors emphasize that 'entrainment can occur only if stimulation frequency is precisely matched to the endogenous rhythm'[35]. To instantaneously change ongoing neuronal activity at any moment with high fidelity, > 1 V/m is required *in vivo*[36], however, more than 20 V/m is necessary in quiescent brain slices[28].

The success of blinding in human experiments depends on the applied intensity (the higher the intensity the stronger the cutaneous discomfort is)[37,38]. Thus, the mean electrode current density in human measurements is 0.03–0.06 mA/cm^2 (1 mA peak intensity, 35 cm^2 anode surface)[39], because it is assumed to be effectively blinded. Using realistic head models, *in silico* studies predict that the aforementioned intensity can induce 0.2 – 0.5 V/m electric fields in the human brain[39]. Different groups attempted to validate the results of modeling using *in vivo* intracranial recordings in humans and found similar values[40–42]. Unfortunately, the orientation of intraoperative recording electrodes (either penetrating or tangential surface mesh types) is not optimal to measure the electric field accurately in these studies, therefore, further measurements are required to validate *in silico* results.

Electrode montages, electrode sizes

A typical montage uses an 'active' and a 'return' electrode. The 'active' electrode is placed over the targeted brain region whereas the 'return' electrode can be positioned in cephalic or extracephalic locations[24,43]. In general, increasing distance between stimulation electrodes on the head can reduce the shunting effect of scalp and eventually can increase the amount of current entering the brain[44]. However, the overall effect of TES always depends on the position of both electrodes, because the placement of electrodes determines the current flow through the cortex[24]. In contrast to many experimental and clinical applications, one cannot assume that brain modulation can occur only under the 'active' electrode, especially when both the 'active' and 'return' electrodes are placed over the head in which case both electrodes are 'active'. One of them acts as an anode and the other one as a cathode; therefore, the two stimulating electrodes cannot be examined separately[24].

The most common electrode configuration in rodent experiments, places an 'active' electrode on the skull and a 'return' electrode on the body[45,46]. This setup can provide a relatively uniform electric field throughout the brain. Alternatively, both electrodes can be applied to the skull which can result in an electric field spectrum between the electrodes[47–49]. The average stimulation electrode surface is ~3.5 mm^2 due to space constraints of the small size of rodents' brain. A striking difference between animal and human montages is the location of stimulation electrodes relative to the skin. To date there are only two rodent experiments that placed the stimulation electrodes over the skin[34,50], the rest of the studies either put the electrode below the skin (epicranial) or halfway through the skull (for a review see[33]).

In clinical studies, the stimulation electrodes are always placed over the skin. The area of the most frequently used human electrodes is 35 cm^2 (7 by 5 cm)[5]. Large rectangular electrodes will induce diffuse, non-focal electric fields in the human cortex. It is safer to use large electrodes due to their smaller current density[51]. Counterintuitively however, smaller electrodes (16 cm^2) were found to reduce cutaneous sensations which is one of the most common side effects of TES[52]. In addition, even smaller electrodes (1.4 cm^2) in a 4x1 ring configuration (so called 'high-definition tDCS [HD-tDCS]') can increase spatial focality in the cortex[39]. Using HD-tDCS, focality refers to the ability to restrict the high intensity region to a smaller target volume in the cortex. In order to achieve focality in depth, Grossmann et. al. (2017) applied temporal interference (TI) stimulation in mice and was able to recruit hippocampal neurons but not overlying cortical neurons. The

indirect results are promising in this study, however up until now no direct evidence could be gained on the spatially restricted effect, and it does not address the issue of weaker, less effective field gradients compared to animal studies, due to the maximally tolerable intensities in human subjects. Innovative engineering solutions can help us to overcome the limitations of TES (poor spatial focality or subthreshold effects), however, we must seek new stimulation techniques that can be translated into human applications.

Stimulus waveform (tDCS and tACS)

Currently several different stimulus waveform profiles are used in animal and human studies, with the overwhelming dominance of two of them: transcranial direct current stimulation (tDCS) uses a constant current and transcranial alternating current stimulation (tACS) which applies a sine-wave stimulus waveform. The instantaneous electric field distribution is similar in both tACS and tDCS, because of the quasi-static approximation at the applied frequency regime; the dielectric properties of tissues are mostly ohmic below 5 kHz[12]. Consequently, both DC and AC stimulation can alter the transmembrane potential of neurons. The effect is linearly proportional to the applied current intensity, but AC stimulation will cause frequency-dependent sinusoidal fluctuations of the membrane potential alternating in two directions from baseline[53,54]. Based on *in vitro* and *in silico* results; the cumulative effect of tACS is the largest when the frequency of stimulation is matched with the frequency of the ongoing brain oscillation[35,54,55]. Besides of local field-potential oscillations, low frequency tACS (0.8 – 1.7 Hz) can also entrain neuronal spiking in widespread brain areas[36,48]. To date, there were only 7 *in vivo* animal studies that investigated the neuronal response to tACS because it is still challenging to measure the brain activity reliably during stimulation[36,48,56–59], especially when the stimulation frequency is close to the frequency of targeted neuronal activity[60].

To overcome this challenge, human studies adopted an intervening recording-stimulation protocol, in which EEG is only recorded before and after stimulation[60,61], and are limited to focus on the lasting post-stimulation neurophysiological aftereffects and/or on induced behavioral changes. Little is known about how tACS can alter ongoing brain activity in humans. In order to analyze the neuronal signal during tACS different artefact removal techniques were developed (e.g. subtraction of principal components, template subtraction, temporal filtering or beamforming[62,63]). All of them are based on the theory that the tACS-induced artefact is linearly imposed on the neurophysiological signal and are stationer at least over several cycles of stimulation. Although, Noury et al.

demonstrated that the detected spectral changes in neural activity at the stimulation frequency could be due to incomplete artefact removal[64]. Therefore, one should be extremely careful when the stimulation frequency is within the range of the frequency of targeted brain oscillations because the presence of residual artefacts can lead to false positive results[64], especially when the stimulation artefact is orders of magnitude larger in amplitude than the neuronal signals to be detected.

One solution could be to apply stimulation at a frequency that is not in the frequency range of interest and measure cross-frequency or phase-amplitude coupling of neural oscillations, however the nonstationarity and waveform distortions of the artefacts can still induce harmonic artefacts that corrupt the observed signals. In conclusion, both stimulation and recording hardware should be further developed to suppress tACS-induced artefacts and allow analysis of neuronal signal during stimulation.

Safety

TES is a safe tool to perform neuromodulation if appropriate protocols are followed[65]. Average electrode current density [A/m^2] is the most commonly used safety parameters for dosing guidelines[66]. The dose of TES is defined by the electrode montage (electrode size and position) and by the intensity (in mA) and duration (in minutes) of stimulation. Note, that a typical clinical session applies stimulation for at least 10 minutes.

Liebetanz at al. found that, brain damage occurs in rats during cathodal tDCS applied at 143 A/m^2 electrode current density (0.5 mA for 10 min, 42 V/m cortical electric field)[45], however other groups reported different values as a safety threshold (61 and 23 V/m electric field; Fritsch and Jankord unpublished data)[65]. A recent study observed lesions using anodal tDCS at 20.0 A/m^2 electrode current density[33]. What could be the explanation of the difference between anodal and cathodal stimulation?

Electrical current generates heat in tissues which in turn can induce brain damage[66]. The induced heat depends on current density linearly, however, it takes time to change the temperature of tissues and it is always altered by local blood flow and metabolism. Due to these latter factors, damage threshold is polarity dependent[66].

The applied current must pass through several different tissues to reach the brain; therefore, it is better to use average brain current density than average electrode current density to predict the volume of damaged brain tissue[67]. Indeed, brain current density depends not only on the electrode current density, but also on individual anatomy, electrode size and position[39].

Considering the differences between animals and humans the usefulness of these safety studies is unclear. However, the lowest threshold for brain damage (20 A/m^2) is still ten times higher than the typical electrode current density used in clinical studies (0.28–2.0 A/m^2)[38]. To date, the most severe side effect was skin lesions in healthy volunteers, which were most likely caused by poor skin-electrode contact[68]. In addition, itching, tingling, headache, burning sensation and discomfort are the most common adverse effects of TES[69].

Overall, TES is a safe tool, however, the rise of do-it-yourself (DIY) brain stimulation communities may increase the risk of electrical stimulation induced self-harm[70]. In most of the cases, DIYer people build their own stimulator and chose stimulus parameters (intensity, polarity, electrode size and position) based on blogs and websites dedicated to the topic[71]. The public is advised to use TES carefully because scientists are still trying to understand the mechanisms of electrical stimulation. Obviously, there is still a lot to learn about intensity, polarity, electrode size and position.

Instantaneous effects of electric field

Despite two decades of intensive research, the mechanisms of action of long-term TES is still not fully understood. As the general readout of the neuronal activity by its target peers is the sequence of action potentials and the released neurotransmitter[72], the main goal of neuromodulation in order to establish instantaneous control on brain activity is to induce or prevent spiking with high fidelity. Since the generation of action potentials have a probabilistic nature[72], the stimulus induced extracellular potential gradients can only bias the probability distribution of this Poisson process. This implies that there is no absolute threshold for field intensity that is minimum required to induce the emission of an action potential; even the weakest stimulus can trigger a spike if the neuron is depolarized enough, however this will still have a low probability, and arbitrarily delivered stimulus pulses will succeed only with a low probability. Still, in terms of this success probability which defines the reproducibility or reliability of the intervention, meaningful threshold levels can be defined, such as the intensity required to emit a spike in 50% of the attempts, or the intensity for an anytime success (i.e. that is strong enough to emit a spike even in the most possible hyperpolarized state of the given neuron). The embedded nature of the neurons into networks makes them even more resistant to external impacts, which increases the robustness of endogenous information transfer, but makes external control even more difficult[73]. *In silico* models suggest that the induced

intracerebral gradients of the weak transcranial direct current stimulation used in clinical studies are far below these thresholds, however even if they are not capable of reproducibly altering the temporal patterns of neuronal activity, they still have some cumulative effect on behavior if applied for long enough periods (i.e. for tens of minutes). The underlying physiology of the cumulative effect of weak stimuli is still under heavy debate and is not in the focus of the current thesis. However, it is worth to mention that there is ample evidence on the role of the stimulation of the peripheral nerves, glial interactions and even placebo effect besides of the direct neuronal modulation.

On the other hand, as I mentioned earlier, animal studies apply much higher intensities which can lead to acute entrainment of neuronal activity both *in vitro*[27,28,74] and *in vivo*[36,48]. In the next section I discuss that under which circumstances is the instantaneous alteration of neuronal activity more beneficial than gaining a delayed effect through long lasting stimulation, and how is it achievable *in vivo*?

Immediate neuronal effects of TES

Besides of particular experimental arrangements to investigate specific scientific questions, there are several conditions, e.g. epilepsy when the application of long minutes of subthreshold stimulation to achieve the termination of seizures is simply meaningless. More broadly, in any cases, when one wants to interfere with ongoing brain rhythms in a phase-dependent manner (i.e. to cause a temporal interference), the stimulus effect must be built up and turned off in cycles of only tens of milliseconds or less. Berényi et. al. (2012) showed that high-intensity, brief gaussian pulses (~6-8 V/m electric field in the brain, 50 ms duration) in a closed loop manner can take over the control on neuronal spiking, can stop ongoing seizure activity and can restore normal brain function. Ozen et. al. (2010) showed that 1 V/m electric field is necessary to modulate the ongoing neuronal activity in widespread cortical areas *in vivo* with good reproducibility. According to *in vitro* studies, such intensity can induce only 0.1 mV transmembrane potential change[75], which is two orders of magnitude smaller than the required depolarization (~15 mV) to elicit an action potential in a resting hippocampal neuron[76].

To resolve this controversy, let me take a closer look at the known mechanisms of TES (both tDCS and tACS) that can lead to immediate changes in neuronal activity.

As I mentioned earlier, DC stimulation is going to lead to neuronal polarization. Models suggest that on one hand, somatic depolarization will directly increase the chance of eliciting an action potential. On the other hand, dendritic hyperpolarization will increase

the cation influx which eventually can elicit bigger excitatory postsynaptic potentials (EPSP's)[26]. These small changes of transmembrane potentials are experienced by a large number of neurons simultaneously, therefore; it can have a significant effect on spike timing[77]. However, the most commonly applied stimulus intensity is 2 mA in human clinical applications, which can generate ~0.45 V/m electric fields in the brain[40,42]. At these intensities tDCS does not have immediate neuronal effects in humans (for a review, see Woods et al., 2016)[78].

In tACS studies, applied current alters the transmembrane potential sinusoidally at the cellular level[53], which is subsequently reflected at the network level, and thereby can modulate oscillations in the electroencephalographic (EEG) recordings, cortical excitability and cognitive processes[79,80]. Fröhlich and McCormick (2010) showed that active neuronal networks can be more sensitive to oscillating electric fields than single cells. I would like to discuss in more details three increasingly robust and deterministic mechanisms that could affect network activity: stochastic resonance, entrainment of neural activity and imposed patterns.

Stochastic resonance is a phenomenon in which adding random noise to a signal can amplify the original signal[82]. In case of tACS, externally applied AC stimulation ('noise') can induce small changes of transmembrane potential of neurons. If the neuron is close to its threshold ('signal'), weak tACS can already bias spike timing. However, it may be difficult to achieve the same effect in each stimulation trials because different neurons may be polarized differently.

Entrainment occurs when neurons become more and more synchronized to a periodic driver (either endo- or exogenous). In case of tACS, spikes will align to certain phases of the externally applied sine wave, which in turn will increase the amplitude of the oscillation at the population level[83]. Entrainment requires higher electric fields than stochastic resonance because the exogenous patterns compete with the endogenous brain oscillations but possesses a certain level of cycle-by-cycle predictivity.

If tACS generates high enough electric fields, one can enforce an arbitrary pattern on a neural network (e.g., imposing theta activity on a network with an endogenous alpha rhythm). These imposed patterns require the strongest electric fields.

Unfortunately, clinical studies use weak electric fields (< 0.5 V/m) therefore little is known about entrainment and imposed patterns in humans. In contrast, researchers regularly apply high intensities (> 5 V/m) in animal models so let me summarize what we know about immediate neuronal effects from *in vivo* rodent experiments.

Acute effects of external electric fields in rodents

Rodent studies typically use ten-fold stronger current intensities compared to humans. Across 28 rodent experiments – where immediate neuronal effects were reported (for a review; see Liu et al., 2018) – the induced intracranial electric fields averaged 6.8 ± 3.8 V/m (n = 11, ten epicranial and 1 subdural studies), compared to < 1 V/m measured/estimated in human TES studies[40–42].

Ozen et. al. (2010) found that 1 V/m is the lowest electric field sufficient to deterministically modulate the timing of spiking activity in widespread cortical and hippocampal areas, however; higher intensities were required to reliably affect local field potentials (LFP) and the membrane potential in intracellularly recorded neurons *in vivo*. Similarly, high electric fields were required to modulate LFP oscillations in urethane-anesthetized rats[59,85]. In addition, these intensities can elicit paw movements or modulate the initiation of endogenous slow waves and their propagation[58,86]. Besides of altering physiological oscillations, more than 1 V/m electric fields can terminate thalamocortical spike and wave patterns in rats[47,48].

In summary, rodent studies demonstrate the physiological effects of high-intensity TES on spike timing, LFP oscillations, and terminating seizure patterns. Achieving similar acute effects in humans is challenging because of many technical constraints.

Technical issues

Invasive recording of the neuronal activity has very limited accessibility in humans; therefore, studies observe the alteration of brain activity in EEG recordings and psychophysiologic observations. Only a few studies recorded the EEG activity simultaneously with the application of tACS. The reasons lye in a technical bottleneck: animal studies suggest that the strongest acute effect, if any, is expectable when frequencies similar to the endogenous rhythms are applied[60,62]. The maximally applicable intensity is limited by the peripheral side effects thus constrains studies to frequency-matched designs. However, extracting the ongoing brain oscillations and remove all stimulation induced artefacts in the exact same frequency regime is impossible in most cases; first, artefacts are orders of magnitude higher than the recorded brain oscillations. For instance, the amplitude of alpha waves is around 100 μV over the occipital lobes but a 2-mA tACS can induce artefacts over 1 V. If an algorithm fails to remove all the artefacts of the induced waveform, that otherwise have very similar features to the endogenous rhythms, it can lead to false positive results and misleading conclusions[87].

Conclusively, if the stimulation frequency matches the endogenous oscillation frequency, which is a prerequisite of causing a low-intensity driven resonance, it is unlikely to recover the artefact-free brain activity, even if the algorithm can almost perfectly clear the recorded signals[64]. Alternatively, one may apply higher intensities at different frequencies, and modulate brain rhythms through the mechanism of imposed patterns, similarly to rodent results. Unfortunately, higher stimulus intensities will more likely saturate the recording amplifiers, thus preventing the analysis of the endogenous LFP during stimulation. In addition, application of higher intensities (> 2 mA) with conventional methods is inducing serious adverse effects including pain or skin erosion under the electrodes.

Aims of the research

The primary goal of my research was to gain a better understanding how TES induced electric fields can affect neuronal activity instantaneously both in rats and humans. We attempted to identify and validate electrical stimulation parameters that are necessary to deterministically modulate ongoing brain activity both in rodents and humans. To accomplish these aims, my project focused on the following tasks:

1. To measure the trans- and subcutaneous electrical stimulation induced electric fields in rats.

2. To determine the electric field necessary to affect single unit activity and membrane potential in anaesthetized rats.

3. To examine how rodent results can be translated into human applications.

4. To design a measurement and stimulation protocol in which TES can alter ongoing neuronal activity in humans. To validate this protocol in rats.

Results

Comparison of sub- and transcutaneous electrical stimulation in rats

In vivo rodent experiments demonstrated that electrical stimulation can elicit stimulus-locked firing of neurons in neocortex[36], can alter the amplitude of intracerebrally recorded local field potentials[48] or can interfere with pathological oscillations[47,48]. However, 90% of the rodent studies placed the stimulation electrodes on the skull not on the skin[84]. The presence of soft tissues can reduce the amount of currents that enter the brain, and the question arise; whether currents of sufficient magnitude even reach the cortex to alter neural activity[88]. Therefore, we examined how skin and head musculature surrounding the skull can influence the magnitude of induced electric fields in the rodent brain. Using 32-channel silicon probes we measured the intracerebral voltage gradients and applied current to the shaved scalp (transcutaneous TES, Fig. 3a) then to the parietal bone (subcutaneous TES). Transcutaneous TES through the same size of electrodes resulted in an $80 \pm 5\%$ current loss, independent of the stimulus intensity (Fig. 3b, c; transcutaneous stimulation: 2.14 (IQR = 1.9–2.44) mV/mm/mA; subcutaneous stimulation: 17.01 (IQR = 14.96–20.85) mV/mm/mA; $P < 0.001$; paired t-test; $n = 20 \times 2$).

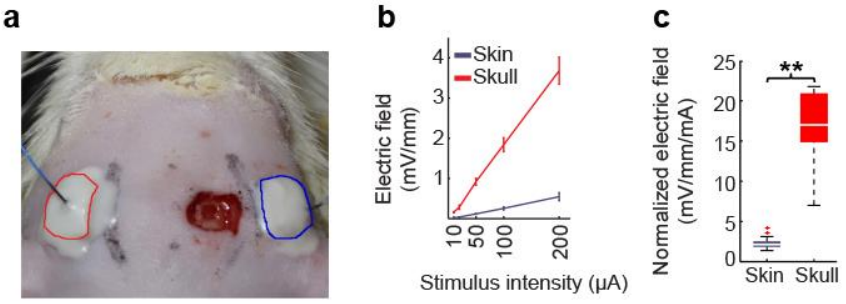

Figure 3. Electric field magnitude during sub- and transcutaneous stimulation in rat
a Photograph of scalp stimulation electrodes and the small hole in the skull through which extra-/ intracellular recordings were made. **b, c** Transcutaneous stimulation at the same stimulus intensities generated several-fold weaker electric fields compared to subcutaneous stimulation ($P < 0.001$, $n = 20$ in 4 rats).

In a more direct physiological comparison, we tested the effects of externally applied direct currents on the intracellularly recorded transmembrane potential (V_m) and spiking of neurons in the deep layers of the visual cortex (Fig. 4a–d). Subcutaneous (skull) stimulation exerted clear and predictable effects on V_m. Depending on the polarity of the stimulation, V_m became depolarized or hyperpolarized in a relatively linear manner (Fig. 4a; Pearson's linear correlation, $R = 0.86$, $P = 0.002$ for transcutaneous and $R = 0.97$, $P < 0.001$ for subcutaneous stimulation, $n = 13$, each), and decreased or increased the

number of action potentials, respectively (Fig. 4b; Pearson's linear correlation, $R = 0.80$, $P = 0.007$ for transcutaneous and $R = 0.95$, $P < 0.001$ for subcutaneous stimulation, $n = 13$, each). Subcutaneous depolarizing pulses significantly decreased V_m (paired t-test with Bonferroni correction; $P < 0.001$ for 400, 600, 800 μA vs. 0 μA; $n = 25$ membrane potential difference values), increased firing rate (paired t-test with Bonferroni correction; $P = 0.001$, < 0.001, < 0.001 for 200, 600, 800 μA vs. 0 μA; $n = 25$ firing rate difference values) and reduced V_m power in delta frequency band (1–5 Hz; +600 to +800 μA, Mann–Whitney U-test with Bonferroni correction; $P < 0.005$, $n = 30$ power value pairs at each frequency bin), indicating that subcutaneous stimulation affected many other neurons as well (Fig. 4c). Hyperpolarizing pulses exerted opposite effect with similar magnitudes on V_m (paired t-test with Bonferroni correction; $P = 0.003$, 0.004 and 0.046 for −800, −600, −400 μA vs. 0 μA; $n = 25$ membrane potential difference values) and reduced firing rate (paired t-test with Bonferroni correction; $P = 0.044$, 0.028 for −800 and −600 μA vs. 0 μA; $n = 25$ firing rate difference values). Using the same current intensities, transcutaneous (scalp) stimulation produced much smaller and more variable effects (V_m was affected at anodal 400–800 μA but not by cathodal pulses; paired t-test with Bonferroni correction; $P = 0.044$, 0.008, and 0.003 for 400, 600, and 800 μA vs. 0 μA; $n = 40$ membrane potential difference values, and even the highest current intensities failed to affect delta power V_m or higher frequencies (Fig. 4d; Mann–Whitney U-test with Bonferroni correction; $P > 0.05$; $n = 35 \times 150$ spectral amplitude values for all conditions). Spiking activity by transcutaneous stimulation was affected at only 800 μA depolarizing pulses (paired t-test with Bonferroni correction; $P = 0.046$ for 800 μA vs. 0 μA; $n = 35$ firing rate difference values), corresponding to intracranial fields of approximately 2 V/m (Fig. 4b, d). In summary, either transcutaneous (skin) or subcutaneous (skull) electrical stimulation can affect spiking activity if the intracerebral electric field is high enough (> 1V/m), but stronger fields are needed to affect network oscillations.

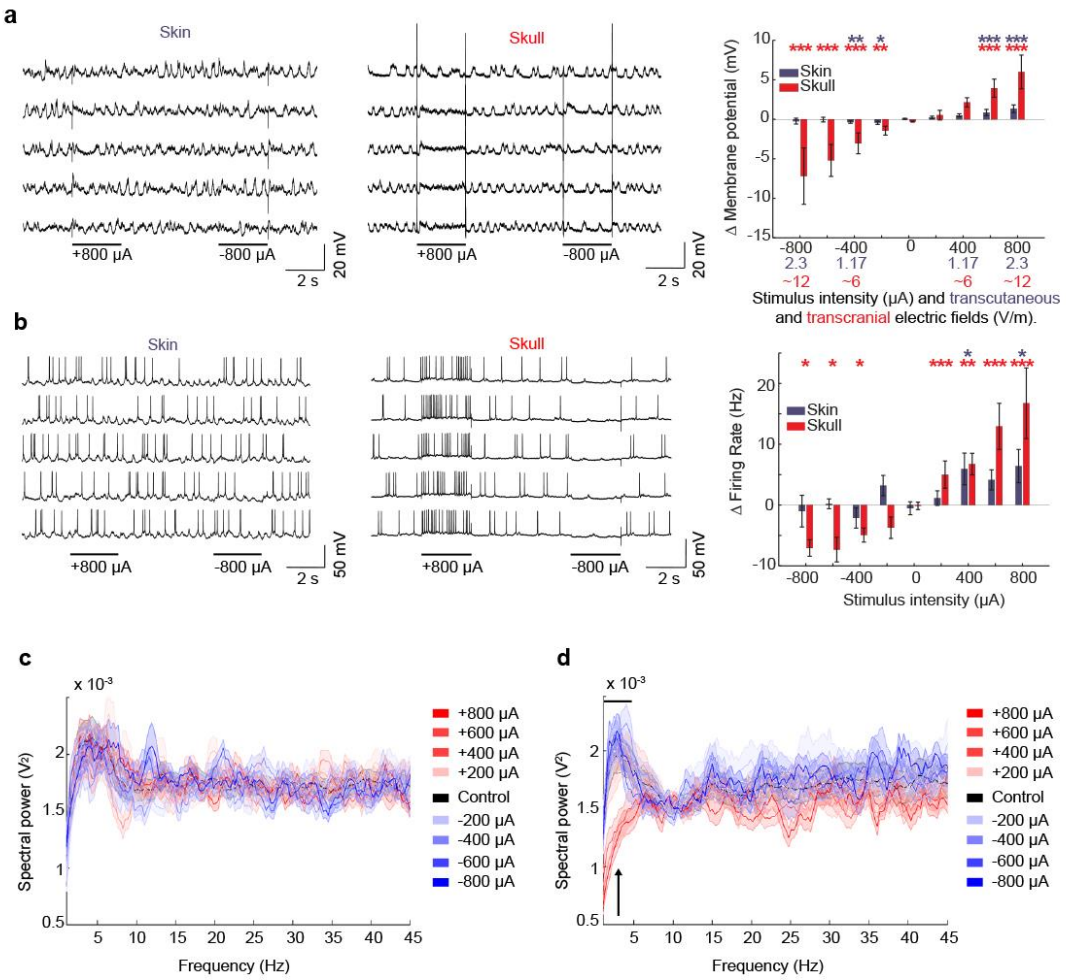

Figure 4. Modulating neuronal activity by subcutaneous or transcutaneous stimulation.

a Subthreshold membrane potential changes of cortical neurons by transcutaneous and subcutaneous direct current stimuli. V_m was held below spiking by intracellularly injected hyperpolarizing current. Five representative trials are shown for each arrangement. Right panel, group effects ($n = 40$ trials from 8 neurons of 3 rats for transcutaneous and $n = 25$ trials from 5 neurons of 4 rats for subcutaneous experiments). Note linear changes of V_m with changing polarity and amplitude of forced fields ($R = 0.86$, $P < 0.005$ for transcutaneous and $R = 0.97$, $P < 0.005$ for subcutaneous stimulation, $n = 13$ trials, each; asterisks mark significant differences against control condition, $n = 25/40$ for subcutaneous/transcutaneous trials). For each stimulus intensity, the generated electric field strengths are shown at the bottom of the plot in blue and red for transcutaneous and subcutaneous stimuli, respectively. **b** Same as **a** but for affected spiking frequency by applied fields ($R = 0.80$, $P = 0.007$ for transcutaneous and $R = 0.95$, $P < 0.005$ for subcutaneous stimulation, $n = 13$, each; asterisks mark significant pairwise differences against control condition, $n = 25/35$ for subcutaneous/transcutaneous trials). **c, d** Changes of V_m power spectra in response to transcutaneous (**c**, $n = 35$ trials) and subcutaneous (**d**, $n = 30$ trials) stimuli. Note the lack of a significant effect with transcutaneous stimulation and prominent decrease of delta power (1–5.4 Hz) at +600 and +800 µA conditions compared to control (arrow; $P < 0.005$, $n = 30$ power value pairs at each frequency bin from 6 animals; Mann–Whitney U-test with Bonferroni correction).

Measuring current spread through scalp, skull and brain in human cadavers

Currently, the best estimates of the stimulus intensities and electrode arrangements needed to induce electric fields of a certain strength intracranially are offered by *in silico* modeling of the human head[41]. As an alternative to modeling, we carried out high spatial density, 3-D intracerebral measurements in cadaver brains in situ (n = 11). Prior to each experiment, the subdural space was filled with physiological saline (0.9% NaCl) solution to replace the cerebrospinal fluid lost during the insertion of the recording electrodes. Thirty-six custom-made multisite electrodes (three to seven sites per electrode, 198 in total, Fig. 12a) were inserted into the brain through holes drilled through the calvarium after removing the soft tissue around the skull (Fig. 12b, c) to create a 3-D montage. As the overall volume of the removed skull was negligible compared to the total skull volume, and the polyimide electrode shafts were tightly sealed, the conduction/isolation properties of the skull were not affected. A needle electrode placed into the sagittal sulcus on the forehead served as the reference electrode. Four or seven pairs of Ag/AgCl stimulation electrodes were fixed to the skull surface bilaterally by conductive electrode gel (Fig. 12c). Applying AC stimulation, the highest electric fields occurred in the neocortex near the stimulation electrodes (Fig. 5a). The relationship between applied current or voltage and the measured electric fields was linear (Fig. 5b; Pearson's linear correlation; $R = 0.52$; $P < 0.001$; $n = 48$). The frequency of stimulation had only a small effect on the magnitude of the induced fields (Fig. 5c; one-way ANOVA; $P = 0.99$; $F(8, 891) = 0.06$; $n = 900$ trials from 5 cadavers). These results confirm the ohmic properties of the brain[19], the surrounding skull, and soft tissue with negligible capacitive components[89]. As expected, larger size electrodes induced larger electric fields (Fig. 5d, case 1: 0.94 ± 0.041, 1.25 ± 0.05, 2.84 ± 0.097 V/m, $P < 0.001$ for all comparison; and case 2: 0.23 ± 0.01, 0.32 ± 0.017, 0.43 ± 0.09 V/m, $P < 0.001$ for all comparison; mean ± SEM; $n = 60$ gradient values)[90].

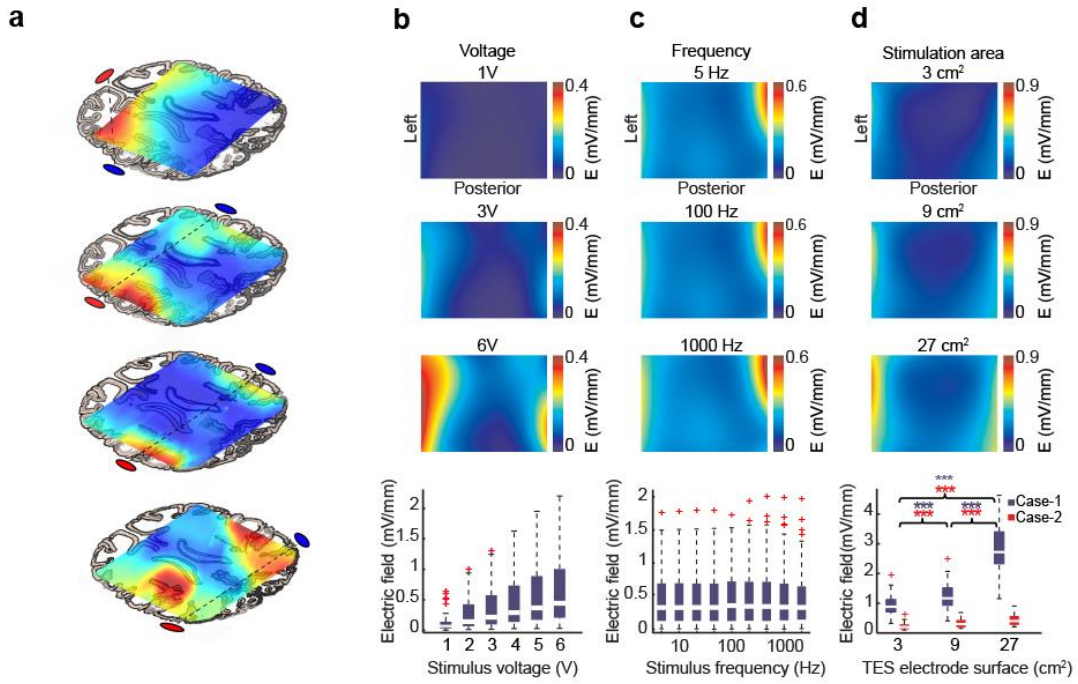

Figure 5. Measuring induced intracerebral electric fields in human cadavers. **a** The effect of different stimulation electrode configurations on the distribution of electric field displayed on a single horizontal slice. **b–d** Effect of stimulus intensity, frequency, and electrode size on intracerebral voltage gradients, respectively. Top three panels denote example gradient maps in the horizontal plane, bottom graphs show population data. **b** Electric field strength is a linear function of applied stimulus intensity **c** Stimulus frequency between 5 and 1000 Hz has a minor effect on intracerebral gradients. **d** Increasing electrode size increases the magnitude of electric fields.

Figure 6 presents comparisons between transcutaneous (scalp), subcutaneous (skull with scalp removed), and direct epidural stimulation results. Transcutaneous experiments used a limited set of recording electrodes (Fig. 6a; one plane of the 3-D matrix, total of 28 contact sites on four or six electrodes in 6 cadavers) introduced via small individual incisions of the otherwise intact scalp. The voltage–current relationship remained linear for transcutaneous stimulation as well, but the slopes were strongly reduced (Fig. 6b; Pearson's linear correlation; $R_{subcutaneous} = 0.92$ and $R_{transcutaneous} = 0.86$; $P < 0.001$ in both cases; $n = 14$ and 81 for transcutaneous and subcutaneous conditions, respectively). Comparison of the current - electric field relationships indicated that approximately 2 mA subcutaneously applied current was sufficient to induce a ~1 V/m field maximum (Fig. 6c; Pearson's linear correlation; $R = 0.56$; $P < 0.001$; $n = 29$). In contrast, the current vs. electric field slope was decreased three-fold when current was applied to the scalp rather than to the skull (Fig. 11c, d; $E_{subcutaneous}(V/m) = 0.41 \times I(mA) + 0.15$; $E_{transcutaneous}(V/m) = 0.13 \times I(mA) + 0.04$).

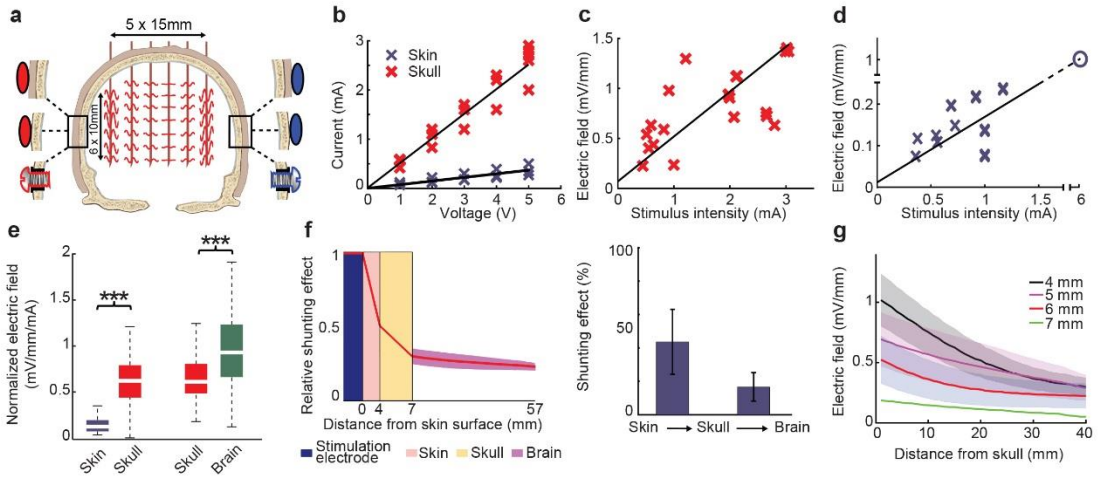

Figure 6 Skin and subcutaneous soft tissue diffuses scalp-applied current in cadaver brains.
a Schematic of the experimental arrangement for transcutaneous, subcutaneous, and epidural stimulation. Example signal traces recorded in a coronal plane. **b** Both transcutaneous and subcutaneous stimulation show intensity-independent linear (ohmic) properties, which allows the calculation of voltage–current relationship. **c, d** Subcutaneous stimulation elicited several-fold larger intracerebral gradients compared to transcutaneous stimulation. Extrapolation from the measured data indicates that approximately 6 mA transcutaneous current can induce 1 V/m intracerebral electric field (circle). Raw data and fitted lines are shown. **e** Ratios of induced intracerebral fields and stimulus amplitude in transcutaneous vs. subcutaneous, and subcutaneous vs. epidural stimulation. **f** 58 ± 7% of the applied current is shunted by skin and soft tissue and a further 16 ± 8% is attenuated by the skull. **g** Effect of skull thickness on induced fields.

Extrapolation of transcutaneous stimulation results suggested that approximately 6 mA current applied to the scalp would be needed to reach 1 V/m voltage gradient in the living brain (Fig. 6d; Pearson's linear correlation; $R = 0.80$; $P < 0.001$; $n = 16$). Across all experiments in which scalp, skull, and epidural stimulations were tested ($n = 6$), we could establish that 58 ± 7% of the current applied through the scalp diffused through the soft tissue surrounding the head. Another 16 ± 8% of the current was attenuated by the resistance of the skull, whereas current spread effectively in the brain, including the meninges, vasculature, ventricles, gray matter, and white matter (Fig. 6e, f; 0.12 (IQR = 0.07–0.19) and 0.62 (IQR = 0.44–0.79) mV/mm/mA for transcutaneous vs. subcutaneous comparison; 0.61 (IQR = 0.49–0.80) and 0.93 (IQR = 0.67–1.23) mV/mm/mA for subcutaneous vs. epidural comparison; paired t-test; $P < 0.001$ in both comparisons; $n = 36$ and 60 for the two comparisons, respectively), supporting the view that the brain is an effective volume conductor[91]. Skull thickness was a potential factor in attenuation of the current spread, explaining some of the variability across subjects (Fig. 6g; Pearson's linear correlation; $P = 0.008$; R^2 adjusted = 0.046; $n = 128$ electric field strength and skull thickness value pairs).

The experiments on the cadaver brains were performed from 3 to 8 days after death. Desiccation measurements of brain specimens revealed that the postmortem age had little effect on the hydration level of the brain (Fig. 7 table). However, previous papers reported that the conductivity is decreased in the postmortem skull and soft tissues[92,93]. Overall, our measurements in human cadavers demonstrate that a significant fraction of the scalp-applied current is lost due to the shunting effects of the skin and soft tissue and the serial resistance of the skull. Approximately three quarters of the current was attenuated across the scalp and skull. These findings were further supported by measuring the induced voltage gradients first in vivo, followed by identical measurements up to 5 postmortem days in chronically implanted rats (n = 3; Fig. 7a).

#	Post mortem age (day)	Brain water (%)
2013 – 18	3	80.37
2013 – 19	6	81.56
2013 – 20	8	78.29
2013 – 21	7	81.01
2014 – 2	5	82.57
2014 – 3	5	82.94
2015 – 2	4	78.95
2015 – 3	7	83.15
2015 – 6	3	86.36
2015 – S1	6	83.33
2015 – S2	7	-
Alive		77 – 78

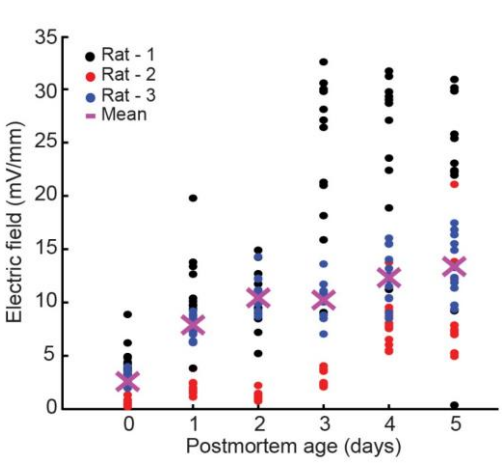

Figure 7 Comparison of cadaver and in vivo conditions
Table Cadaver brains did not go through significant desiccation after death. For comparison, literature value for *in vivo* hydration level is shown, too ('Alive'). **a** Comparison of in vivo and post-mortem conditions in rats. Induced voltage gradients in vivo and 1 to 5 days after death.

Affecting human brain network activity by ISP stimulation

Our human cadaver and *in vivo* rat measurements indicated that approximately 6 mA currents applied to the scalp are needed to effectively alter ongoing neuronal activity in humans. To deliver stronger currents to the brain we need to minimize peripheral and indirect effects; and we should be able to record the brain activity and stimulate simultaneously. Our proposed solution uses spatio-temporally rotating *I*ntersectional *S*hort *P*ulse (ISP) stimulation (Fig. 13), in which current is delivered through multiple sequentially activated pairs of stimulation electrodes by rapidly switching (μs scale). An added advantage of fast pulse stimulation is that the transients of high frequency pulses

affect simultaneously recorded neuronal activity substantially less than conventional tACS and they do not saturate recording amplifiers even at relatively high intensities.

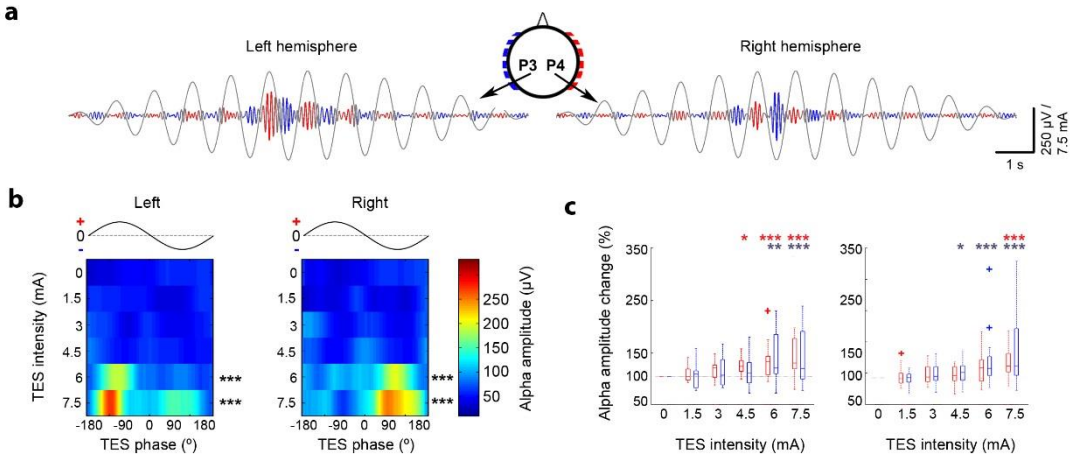

Figure 8. ISP stimulation of the scalp phasically modulates ongoing brain oscillations in human subjects.
a An example trial demonstrating alpha amplitude increase for high-intensity ISP stimulation. Alpha-band filtered EEG signals are color coded based on the instantaneous ISP phase for better visibility; blue and red colors denote stimulus trough (right-to-left currents) and peak (left-to-right currents), respectively. Gray sinusoids denote the ISP stimulus epoch with an increasing – decreasing amplitude. **b** Phase modulation of the alpha amplitude by ISP stimulation for the entire session from the same subject as shown in **a**, showing intensity-dependent alpha amplitude increase. Note the alternating phase modulation of the left and right hemisphere-derived EEG signals at 6 and 7.5 mA intensities. Color maps show the phase-dependent median alpha amplitudes. **c** Population analysis for the left and right hemispheres, respectively, revealed an intensity-dependent effect.

To test ISP in humans, a circular array of 12 stimulation electrodes (six on each side; Fig. 8a) was placed around the head and ISP stimulation was applied in 19 healthy human subjects. Each stimulation site consisted of a 0.9% NaCl solution-soaked sponge square connected to 2 × 3 cm copper mesh. Scalp EEG was monitored by a 2-site montage (P3 and P4 against reference Pz). In each session, 1-min long control recordings were obtained before and after the stimulation session (12 min). To avoid onset and offset effects, ISP stimulation consisted of a train of 1-Hz sinusoids with increasing and decreasing intensity (0, 1.5, 3, 4.5, 6, 7.5, 6, 4.5, 3, 1.5, 0 mA per cycle; Fig. 8a, b; Fig. 13) for 12 s, repeated 60 times for each subject. The low frequency (1 Hz) stimulation allowed us to investigate the anodal–cathodal phase modulation of the amplitude of the spontaneous EEG (represented by the dominant alpha band activity) simultaneously in the left and right hemispheres. This approach reduces the possibility that stimulation artifacts and their harmonics contaminate the results[48]. The residual ISP artifacts were removed by an offline subtraction of the stimulation-triggered moving average. The

artifact-removed signal preserved the major features of the unstimulated control brain activity (Fig. 14).

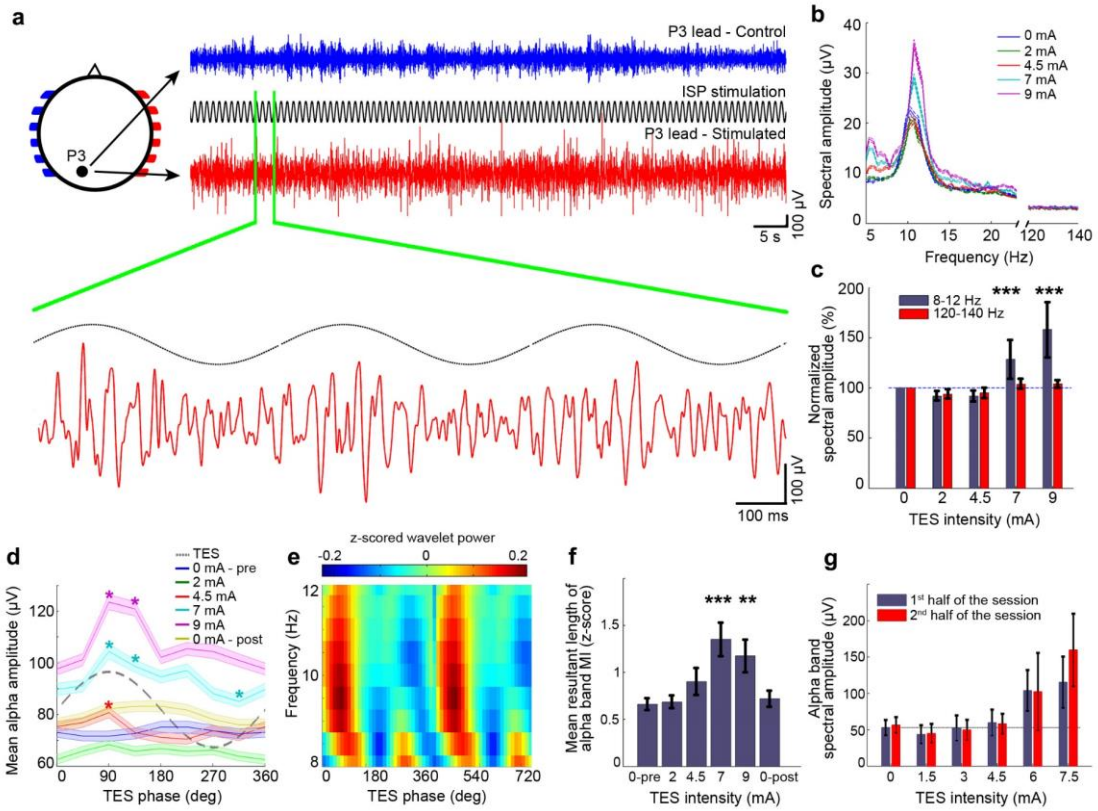

Figure 9. High intensity ISP stimulation of the scalp phasically modulates ongoing alpha waves in human subjects.
a EEG traces are shown during eyes closed condition (control and 7 mA stimulation, blue and red traces). A 3-s magnified segment of EEG trace at P3 lead is also shown. The 1 Hz modulation of the baseline was removed. **b** Single session example of power spectra of EEG traces during increasing ISP intensities at 1 Hz. **c** Quantification of ISP stimulation-induced increase in alpha band power in a single session. The control frequency band (120–140 Hz) showed no significant change. **d** Single session example of alpha wave amplitudes as a function of the phase of 1 Hz ISP sinusoid stimulation. Asterisks denote phase bins significantly different from the mean. **e** Single session example wavelet map (9 mA, 1 Hz ISP) shows ISP phase modulation of the alpha band power. **f** Alpha band power modulation of wavelet decomposed EEG by 1 Hz ISP stimulation phase. **g** ISP stimulation-induced increase of alpha power was stable throughout the recording epochs, as shown by the similar values during the first and second halves of the stimulation sessions.

TES phase modulation of the amplitude of alpha waves became visible by eye on the filtered signal at high ISP intensities (6 and 7.5 mA; Fig. 8a, b; paired t-test with Bonferroni correction; $P < 0.001$ for 6 and 7.5 mA in both hemispheres; $n = 45$ trials). The LFP modulation was present in both hemispheres and alternated in phase, due to the shifting of the anodal - cathodal current direction (compare blue and red epochs in Fig. 8a, b). For group statistics, the mean alpha amplitudes near the stimulus peak (−135° to

−45°) and near the stimulus trough (45° to 135°) were measured separately at P3 and P4 at each current intensity. Significant modulation of the LFP amplitude by the TES phase was observed at current intensities of 4.5, 6, and 7.5 mA at each hemisphere when the preferred current direction was applied (Fig. 8c, paired t-test with Bonferroni correction; left hemisphere at TES trough: $P = 0.006$, < 0.001 for 6 and 7.5 mA; left hemisphere at TES peak: $P = 0.01$, < 0.001, < 0.001 for 4.5, 6, 7.5 mA; right hemisphere at TES peak: $P < 0.001$ at 7.5 mA; right hemisphere at TES trough: $P = 0.01$, < 0.001, < 0.001 for 4.5, 6, 7.5 mA; $n = 1025$ trials for all conditions from 18 subjects. All intensities were tested against the 0-mA condition).

In three of the subjects, we also used step currents of 1 Hz ISP stimulation, instead of the intensity increasing-decreasing ramp. The results of this experiment support those obtained by ramp stimulation (Fig. 9a–f). Current intensity exceeding 4.5 mA increased alpha band spectral amplitude (Fig. 9b–c; paired t-test with Bonferroni correction; $P < 0.001$ for 7 and 9 mA vs. 0 mA; $n = 405$ - 408 power values for each stimulus intensity), and brought about stimulus phase-dependent amplitude modulation of the alpha waves (Fig. 9d–f; two-sample Kolmogorov-Smirnov test; $P < 0.001$ and 0.019 for 7 and 9 mA vs. 0 mA; $n = 16$, 10, 8, 18, 10, and 12 modulation vector length). This experiment also showed that the subjective decrease of the perceived sensory effects over the course of the experiments cannot be attributed to changes in alpha power since alpha power did not change between the first and second halves of the experiment (Fig. 9g; paired t-test; $P = 0.96$, 0.79, 0.44, 0.44, 0.74, 0.11 for 0, 1.5, 3, 4.5, 6, 7.5 mA intensities; $n = 23$ spectral amplitude pairs).

In a separate group of subjects ($n = 6$), we examined whether the EEG changes could be accounted by non-specific sensory stimulation or potential arousing effects of TES. We used current steps (tACS) of 1 Hz ISP stimulation (2 or 6 mA for 5 min with 1-min rest periods; Fig. 10a). To test for the effects of peripheral sensory stimulation, we interleaved the ISP stimulation epochs with a similar protocol, where the adjacent electrode pairs were stimulated with opposite polarity ('shuffled ISP' protocol: first pair received a left–right direction current pulse, second one received a right–left, third one a left–right, and so on; Fig. 10a). Because of the alternating direction of the induced electric fields with the shuffled ISP, the summed effect in neurons was expected to be close to zero. The results with the regular ISP protocol confirmed the hemisphere-specific, stimulation phase-induced modulation of alpha waves (Fig. 10b; one-sample t-test with Bonferroni correction; $P < 0.005$ for left–right and right–left direction 6 mA ISP in both hemispheres;

$n = 809$ power difference values). In contrast, the shuffled ISP induced only minor physiological effects on EEG activity (Fig. 10b; one-sample t-test with Bonferroni correction; $P < 0.005$ for left–right 6 mA shuffled ISP in left hemisphere; $n = 809$ power difference values). Stimulus intensity at 2 mA failed to induce any detectable changes (ISP or shuffled ISP; one-sample t-test with Bonferroni correction; $P = 0.36$, 1.06, 2.22, and 1.45; $n = 809$ power difference values).

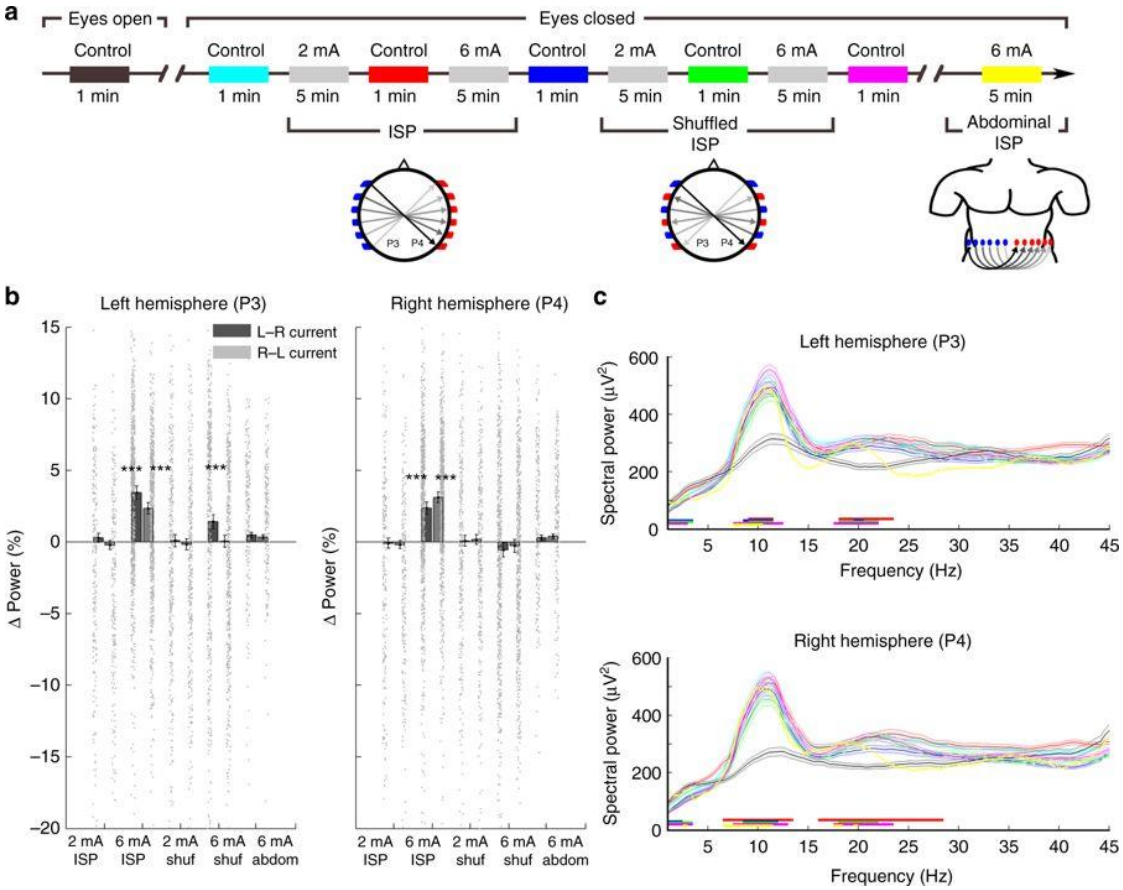

Figure 10. Comparison of ISP and shuffled ISP stimulation on the EEG of human subjects.
a Sequence of the experimental protocol. ISP stimulation used the same arrangement as in Fig. 5. During shuffled ISP, adjacent stimulation electrodes were stimulated with opposite polarity. While shuffled ISP increases local current flow in the scalp, the alternating directions of the induced electric fields ideally resulting in a zero current in the brain. **b** Group results shown separately for the left and right hemispheres. 6 mA current ISP stimulation increased alpha power in both hemispheres. Shuffled ISP exerted only a unilateral and weaker effect. Intensities at 2 mA were ineffective. Abdominal stimulation (6 mA ISP protocol) did not exert a significant effect on alpha power. **c** Spectral power comparison between eyes open control and eyes closed control periods. Horizontal lines indicate significant changes from the eyes open condition. Color coding of the conditions is the same as in **a**.

As an additional control for potential arousal effects, the same subjects were also tested with the same ISP protocol but with the stimulation electrodes placed on the abdominal

wall (Fig. 10a). No hemisphere-specific, stimulation phase-induced modulation of alpha waves was observed in the peripheral control experiment (Fig. 10b; 6 mA abdominal; one-sample t-test with Bonferroni correction; $P = 0.41$, 0.39, 1.68, and 1.18; $n = 809$ power difference values).

Focused TES effect by ISP stimulation

For many clinical applications, it would be desirable to apply TES in a spatially targeted manner and simultaneously monitor the ongoing brain activity to verify online effects. We have seen in humans that applying ISP stimulation makes this latter possible, but can we achieve spatial selectivity using ISP? The scalp, skull, and brain conduct current in a homogenous manner, therefore, simultaneous application of TES through multiple electrode pairs cannot induce a spatially confined effect. However, using our rapidly switching ISP method, each stimulation pair will generate an electric field which will polarize the cellular membrane of neurons in the brain. Because of the short integration time constant of the neuronal membrane (5–20 ms), neurons can temporally integrate the effects of multiple electric fields with similar vector directions (Fig. 11a)[94].

To test our model prediction of focal effect in rats, current pulses were delivered sequentially and in a spatially asymmetric manner through independently programmable isolated current generators, which were connected to a 3-D printed gel-electrode strip glued to the temporal bone surface (Fig. 11b). Unit activity was recorded bilaterally in the CA1 region of the hippocampi with 32-channel silicon probes (7 anesthetized and 1 chronically implanted rat). The hemisphere target of the bipolar stimulation configuration was alternated (Fig. 11b, c; Fig. 15). The effectiveness of the ISP stimulation on spatially targeted entrainment of single unit activity is illustrated for an example neuron from the left hippocampus (Fig. 11c). The artifacts of the short duration stimulation pulses did not affect the recording quality as demonstrated by the similar spike waveforms and spike autocorrelation histograms of the putative single unit during stimulation and stimulation-free periods (Fig. 11c). Of the 127 isolated single units, 55 were significantly affected by at least one configuration of the stimulation protocol (32 increased and 23 decreased, significance threshold: $P < 0.05$; Wilcoxon signed rank test; $n = 300$ firing rate values for each neuron and condition, all tested against baseline condition). To quantify the focusing effect of ISP, we calculated the fold-change of unit discharge in the left and right hippocampus, respectively. Using only three rotating dipoles, the current-focusing effect of ISP resulted in a several-fold increase in induced unit discharge between the targeted

and non-targeted hemispheres (Fig. 11d, 1.8 ± 2.35-fold vs. 1.017 ± 0.63-fold; mean ± SD; $P = 0.001$; Wilcoxon signed rank test; $n = 55$ units).

In four of the above animals (three anesthetized and one chronic; 77 units), the spatial selectivity of the ISP method was compared to traditional direct current (DC) pulses (for DC stimulation, the electrodes in the same hemisphere were short-circuited; the same current intensity was used for DC and ISP stimulation). For each protocol, 500 ms stimulation epochs alternated with 1000 ms stimulus-free epochs using the following sequence: ISP_{left}, ISP_{right}, DC_{left}, DC_{right}. Eighteen (ISP) and ten (DC) neurons showed significant firing rate changes to at least one stimulation configuration (significance threshold; $P < 0.05$; Wilcoxon signed rank test; $n = 340$ firing rate values for each neuron and condition, tested against baseline). Of the 18 ISP-driven hippocampal neurons, eight (44%) responded differentially to ISP_{left} and ISP_{right} conditions (significance threshold: $P < 0.05$; paired t-test; $n = 340$ firing rate pairs for each neuron). Of the 10 DC-driven neurons, only one neuron (10%) showed significant difference to left (anode) vs. right (anode) stimulation (significance threshold: $P < 0.05$; paired t-test; $n = 340$ firing rate pairs for each neuron). In summary, the ISP stimulation affected neural activity in spatially targeted manner, even though skull thickness, brain geometry, tissue anisotropy, and ventricles likely distorted current spread.

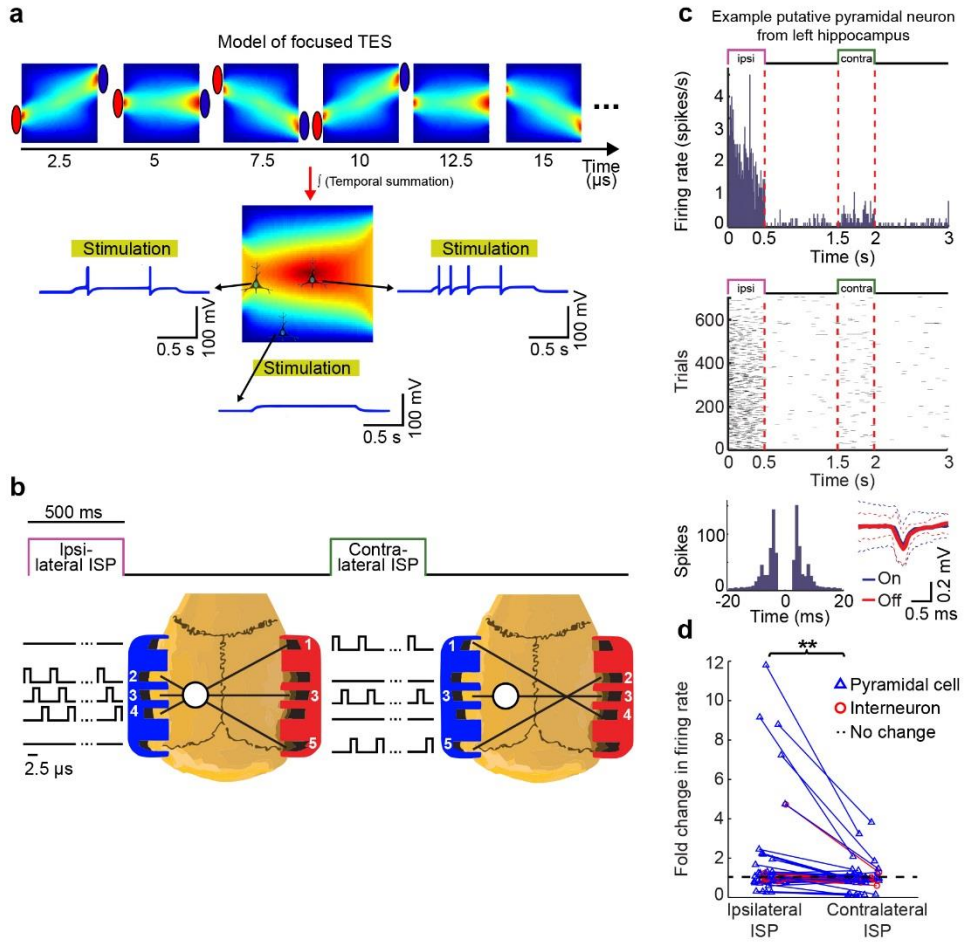

Figure 11. ISP stimulation can spatially focus induced fields.
a Leaky integrate-and-fire neuron model cartoon to demonstrate the concept of ISP stimulation. Stimulus current is delivered sequentially through three independent electrode pairs generating a continuously changing intracerebral gradient pattern. Neuronal cell membranes can integrate these patterns due to their relatively slow membrane time constant (5 - 20 ms). Consequently, neurons at the cross-section of the current flow axes integrate all three stimuli and become more strongly entrained than neurons located outside the focus. **b** Experimental protocol to measure the efficacy of ISP. White circle marks the craniotomy for the example left hippocampal neuron shown in **c**. The contralateral craniotomy is not displayed for simplicity. 3D-printed gel electrode holders (anode = left; cathode = right) were attached to the temporal bones bilaterally with five electrodes on each side. Three electrode pairs were programmed to target the ISP beams on either the left or the right hemisphere. Each electrode pair was pulsed for 2.5 μs and the pulses cycled through the three pairs for 500 ms followed by non-stimulated 1-s control periods. This sequence was repeated to alternatingly stimulate the right or left hemisphere. **c** Response of an example neuron. The putative pyramidal cell from the left hippocampus was strongly excited by the ipsilateral focal stimulation, as shown by peristimulus time histograms (top panels) and raster plots (middle panels). ISP stimulation did not affect isolation of single units as demonstrated by the similar autocorrelation histograms and identical spike waveforms during stimulation and control periods. **d** Fold-changes of normalized firing rates of the significantly modulated cells from the left (n = 32 units) and from the right hippocampus (n = 23 units) show lateralized effect of the ISP stimulation.

Discussion

Using *in vivo* experiments in rodents, we determined the minimum electric field that is necessary to alter the ongoing brain activity – approximately 1V/m. Although this is a very weak field, there were reasons to believe that the currently used stimulation parameters in humans do not reach this threshold. Therefore, we measured the 3-dimensional distribution of the TES induced electric fields in human cadavers, and we found that up to 80 percent of the current applied to the scalp is lost due to the shunting effects of the soft tissue surrounding the skull and the resistance of the skull. To inject higher current intensities into the brain, to reduce the peripheral side effects and to enable simultaneous recording and stimulation, we designed the 'intersectional short pulse' stimulation method. We recorded EEG activity in healthy subjects while applying ISP to the scalp. These experiments demonstrated clearly that at higher current intensities it is indeed possible to modulate the ongoing brain activity. Finally, we demonstrated the spatial specificity of the ISP method in rats.

TES-induced physiological effects

Despite more than 4000 publications (Web of Science) on non-invasive brain stimulation techniques in the past decade, we lack of understanding how TES can affect neurons and can lead to behavioral and/or therapeutical outcomes *in vivo*. It is also unclear whether TES works through direct (change in excitability of neurons) or indirect effects (placebo, activation of peripheral nerves, retina, cochlea, glia, immune system, and blood flow)[84]. In principle, the efficacy of TES depends on a variety of factors including neuronal density and geometry, alignment of dendrites and axons relative to the electric field[53,77], type and distribution of ion channels in the neurons and degree of myelination[95]. These factors must be addressed experimentally because they are different between brain regions and might vary across species[67,84]. Neurotransmitter-induced postsynaptic potentials and ephaptic coupling can affect neuronal excitability. Both mechanisms can influence subthreshold membrane potentials and spiking[8]. When a neuron is about to emit an action potential, even a weak electric field can bias spike threshold. *In vitro* experiments have shown that < 1 V/m oscillatory field can be coupled to intracellularly generated oscillations[8,35]. Whether such weak electric field (< 1 V/m) could result in functional/clinical changes can only be determined by targeted recordings. Especially considering that hippocampal theta oscillations across the CA1 pyramidal layer can elicit voltage gradients of > 4 V/m and > 15 V/m fields are induced by sharp waves[7]. Yet, it is

also important to emphasize that the requirements of affecting spike threshold of some neurons occasionally in wide areas of the brain versus consistently biasing activity of neuronal circuits are different. We attempted to measure the minimum current intensity that can reliably affect local networks in the intact brain. Our *in vivo* intracellular recordings have revealed that > 1 V/m intracerebral electric fields were needed to exert measurable effects on spikes and subthreshold V_m, but several times larger currents were required to measurably affect the associated network rhythms[7,36,48,81,96]. This difference may be explained by the competition between the applied fields and the strong influence of endogenous network patterns.

Current flow through the scalp, skull and brain

In rodent experiments, TES induced electric fields are typically ten-fold stronger compared to human studies[97] and stimulating electrodes are often placed on the skull, the dura mater, or directly on the brain surface[84]. Therefore, translation of animal experiments to humans are extremely difficult. On the other hand, computational methods have become increasingly sophisticated over the years[39,89,98], experimental data are needed to justify the modeling assumptions. Subdural measurements in implanted patients[42] can be useful but limited because they estimate fields tangentially to the cortical surface, whereas the largest voltage gradients are oriented orthogonal to the cortical surface[40]. Using scalp, cranial, and epidural stimulation electrodes and multiple recording electrodes, we quantified the 3-D spread of electric fields in both rodents and human cadavers. Our findings confirm the largely ohmic nature of current spread in the brain[19], skull, and the surrounding soft tissue[89]. The scalp, subcutaneous tissue, and muscles function as an effective shunt, resulting in at least 50% reduction of applied current intensity. The serial resistance of the skull further reduces the current flow by another 10 - 25%, depending on the thickness of the skull[99]. Given the importance of these attenuating factors, the amount of soft tissue, hair, and skull thickness should be taken into account in estimating the magnitude of TES induced intracerebral electric fields[89], and variation of these factors may explain the large individual variability in humans in response to TES[42,100].

ISP: injecting high current intensities and targeting brain regions

Our in vivo rat data – both intra- and extracellular recordings – suggest that in order to alter the ongoing firing rate of neurons, one must generate at least 1 V/m electric field in the vicinity of those cells and even higher electric fields may be needed to phase-entrain brain rhythms to arbitrary stimulus frequencies.

In addition, we estimated from our cadaver experiments that scalp-applied currents should exceed 4-6 mA to achieve 1 V/m voltage gradient in the brain. Electric conductivity of the postmortem tissue may change after death[101,102]; therefore, we compared the *in vivo* versus postmortem induced electric fields in rats and found that larger current intensities must be used in alive animals in order to achieve the same electric fields[93].

Is it possible to reach 1 V/m electric field in the human brain using TES? According to modeling, primate and human studies[40–42,98,103]; the answer is no, if we apply one of the currently accepted, 'standard' TES protocols (2 mA current intensity, 20 cm^2 electrode surface)[65]. Even though there is a linear relationship between applied current and induced electric field, one cannot simply increase the current intensity above 2 mA, because 1) larger than 2 mA currents should be avoided because of the increased risk of pain, burning sensation, phosphenes, and other side effects[65,104,105] and 2) the recording amplifiers will be saturated during TES and prevent the recording of ongoing brain activity during stimulation[78]. To reduce scalp sensation or other side effects, to increase the direct effects of TES on brain activity and to prevent the amplifier saturation[100,104,106–109], novel approaches are needed[86].

To overcome these limitations of 'standard' TES protocols, we developed a new method called 'intersectional short-pulse' stimulation. ISP uses brief and rapidly rotating current pulses via multiple stimulation electrode pairs. In theory, the more stimulation electrode pairs are used, the smaller the adverse effects are on the periphery and other brain regions. In our human measurements, we used six pairs of stimulation electrodes which reduced the required local momentary current by six-fold. ISP was tolerable even at 7 mA current intensities; however, we could not eliminate all the adverse skin effects and vestibular reactions. In addition, the high frequency pulses during ISP stimulation did not saturate the recording amplifiers; therefore, we were able to measure the ongoing EEG activity during scalp stimulation.

Instead of focusing on brain rhythm-entrainment effects[62,83], in which residual artifacts are notoriously difficult to eliminate[64], we examined how the amplitude of the

spontaneous LFP was biased by the slowly changing external fields[48]. This method is similar to applying tDCS at multiple current levels, where the additive/subtractive effect of the applied field can be probed on the amplitude of native network patterns[48]. We have verified the validity of this approach previously in rodents, using both LFP and unit firing[48]. We found that > 4.5 mA currents were required to reliably bias the amplitude of occipital alpha waves. In contrast, when adjacent electrodes were stimulated with opposite polarity in a subset of human measurements (shuffled ISP), no reliable brain responses were detected, even though skin sensation side effects increased. The latter effect may be explained by the stronger current density induced by the opposite polarity of neighboring sites.

While we designed our measurements to maximize the stimulation effects on the parietal–occipital region where alpha waves are of largest amplitude, we cannot exclude the possibility that an improved configuration of stimulation sites could reduce the minimum effective current somewhat further in future studies.

TES might be an alternative treatment option to DBS in several clinical conditions if we could recruit deep-lying neurons without affecting superficial ones. However, spatial focality cannot be achieved in a homogeneous tissue because the electromagnetic wavelength of TES is much larger than the dimensions of the head[110]. It is generally thought that TES cannot limit the high-intensity region to a small target volume[89,111]. A recent study challenged this biophysical view and achieved 'non-invasive DBS' using multiple interfering waveforms[86]. Our modeling showed that ISP can exploit the time-integrating property of the neuronal membrane (i.e., the membrane time constant of neurons is ~20 ms). Using just three rotating dipoles in rats, we demonstrated a proof of principle for the spatial focusing effect of ISP by confining the ISP effect to largely one hemisphere.

An obvious next step in advancing the ISP technique is to increase the number of intersecting dipoles generated by pairs of stimulating electrodes. For example, using a montage of 32 electrodes with highly conductive coupling to the skin, a large number of dipoles can be formed to create a circumscribed 3-D intersectional focus or target two or more brain structures while reducing the locally applied currents, potentially below the skin sensation threshold. Combining 'ground truth' measurements from the human cadaver brain with computational models of the head can lead to a rationale design of focused electric activation of brain structures without adverse and perceivable peripheral effects.

In conclusion, we demonstrate that affecting neuronal circuits directly and instantaneously in the human brain requires higher intensity currents than used in conventional TES experiments. Implicitly, our results also suggest that behavioral and cognitive effects reported in previous tACS studies have likely been achieved by indirect mechanisms on brain activity, which needs to be explored in detail. To achieve sufficient magnitudes of intracranial fields without direct peripheral side effects, novel methods will be required.

Materials and methods

Measurements were performed in the Department of Physiology, Pathology and Neurology, Faculty of Medicine, University of Szeged and the Neuroscience Institute, Langone Medical Center of the New York University. The experiments were approved by the Ethical Committee for Animal Research (ethical permission numbers: XIV/471/2012 and XIV/218/2016), and the Ethical Committee for Human Research (ethical permission numbers: 98/2013 and 164/2014, for the measurements on cadavers and healthy subjects, respectively) at the Albert Szent-Györgyi Medical and Pharmaceutical Center of the University of Szeged in accordance with European Union guidelines (2003/65/CE) and by the Institutional Animal Care and Use Committee of New York University Medical Center IACUC (protocol number: 160926–01).

Experiments on rats

16 female and 3 male Long-Evans rats (350–450 g) and 8 male Wistar rats (250–450 g) were implanted with custom-made recording and stimulating electrodes under urethane anesthesia (1.3 g/kg, intraperitoneal injection) for the extracellular and the whole-cell patch clamp recording experiments, respectively.

Comparison of transcutaneous and subcutaneous TES in vivo

Measurement of TES induced electric fields

For transcutaneous electrical stimulations, a pair of silicon single-pocket electrodes (2-by-2-by-1 mm, 4 mm^2 surface area) filled with conductive EEG gel was glued on both sides of the head of the rats. Small incision was made on the scalp and a 1.2 mm diameter craniotomy was drilled (Fig. 3a). A 32-channel silicon probe (Buzsaki32-H32; NeuroNexus) was inserted in the axis of the stimulating electrodes at 3 mm posterior from bregma and 2 mm lateral of the midline, into the CA1 region of the hippocampus. The craniotomy was sealed with biocompatible silicone (Dow Corning®).

After the transcutaneous stimulation, the silicon probe was removed, and the skin was retracted, and another set of silicon pocket electrode were used on the temporal bone, as described above. The silicon probe was inserted again at almost the same location (2.8 mm posterior from bregma and 2 mm lateral of the midline).

Varying frequencies (10, 100, and 1000 Hz) at varying amplitudes (10, 20, 50, 100, and 200 μA) were used for both settings in current-controlled mode (STG4002; Multi Channel Systems).

The recorded signals ($n = 32$ channels) were amplified (400× gain) and stored after digitization at 20 kHz sampling rate per channel (KJE-1001, Amplipex). To calculate the electric field 500 sinus cycles were averaged for each condition and then the peak-to-peak amplitude was measured for each channel and a mean shank voltage was computed. Finally, we calculated the first spatial derivative of these potential values.

We measured the impedance of all contact sites at 10, 100, and 1000 Hz (Intan recording software, Intan Technologies) and excluded those channels from the analysis whose impedance values were higher than 2 MOhm.

Effect of TES on membrane potential and single unit activity

Yuichi Takeuchi performed these experiments.

A pair of silicon pocket electrodes filled with conductive EEG gel were attached bilaterally on the skin or on the temporal bone of rats for transcutaneous and subcutaneous stimulation, respectively, similarly to extracellular recording experiments. A craniotomy (~2 mm diameter) was made 5.0 mm posterior from the bregma, 4.0 mm lateral of the midline. Patch-pipettes were made from borosilicate glass capillaries (GC150TF-10; Harvard Apparatus) and their tip resistance were 5–7 MΩ when filled with an intracellular solution: (in mM) 135 K-gluconate, 10 HEPES, 10 Na2-phosphocreatine, 4 KCl, 4 ATP-Mg, and 0.3 GTP-Na3 (pH = 7.25, 290 mOsm). Liquid junction potential calculated as +18.6 mV was offline-compensated. The patch-pipettes were lowered perpendicularly with a fine stepper motor and blind in vivo whole-cell recordings were performed from cortical neurons (0.5–1.3 mm from the pia) as previously described[112]. Signals were filtered at 3 kHz and digitized at 20 kHz (HEKA Elektronik). The pipette capacitance, membrane capacitance, and series resistance were compensated. If series resistance varied more than 20% or increased above 50 MΩ, the data were discarded. Direct current stimuli at varying amplitudes (200, 400, 600 and 800 μA) were used (STG4002; Multi Channel Systems). After the whole-cell transmembrane potential recordings, the recorded neurons were detached from the pipette. After reaching a juxtacellular position, the same set of electrical stimuli were recorded extracellularly. To obtain the transmembrane voltage, artifacts were subtracted from intracellularly recorded potentials[28]. Power spectra of the stimulated and control epochs were calculated on a trial-by-trial basis, using fast Fourier transform, before averaging. Spectra were whitened by the 1/f method.

Finally, a 4-shank 32-channel silicon probe (Buzsaki32-H32; NeuroNexus) was inserted in the vicinity of the recorded neuron to record extracellular electric field in response to

the same stimulation as during intracellular recordings. The extracellular recordings were performed as described above and served as a measurement of the induced electrical gradient at the locations of the recorded neurons.

Measuring the effect of postmortem age

Rats were implanted with a pair of silicon pocket electrodes as described above. Twelve holes (0.5 mm diameter) were drilled in the skull and a custom-made 6×2 recording electrode matrix was inserted into the brain. The spacing between the individual electrodes was 2, 1.7, 2.2, 1.7, and 2 mm in the *x* axis and 2 mm in the *y* axis. The electrode matrix was inserted at 3 mm depth in the brain and the craniotomies were filled with silicone (Dow Corning®). Once the silicone dried, the whole skull was covered by dental cement (Duracryl™ Plus) and the skin was closed by sutures to restore its conductive integrity. Subcutaneous tACS was performed in voltage-controlled mode using various stimulation parameters as described above (STG4002; Multi Channel Systems).

After the in vivo measurement, the rats were euthanized by sodium pentobarbital (150 mg/kg, intraperitoneal injection). The corpses were kept at 4 °C after death in plastic bags to prevent desiccation. Subcutaneous tACS and recordings were repeated on postmortem day 1, 2, 3, 4, and 5.

Measurements on human cadavers

Cadavers without known brain disorder were selected for measurements. The corpses were kept at 4 °C after death in plastic bags until autopsy to prevent desiccation. The autopsy theater temperature was 22 °C. The routine medical autopsy procedure was done on the same day as experimental measurements. No cadaver was excluded from the analysis.

Recording tACS-induced intracerebral electric fields

The scalp was cut along the coronal plane connecting the mastoids. The anterior and posterior halves of the scalp were retracted forward and backward, respectively. The temporal muscles and soft tissue were also removed. After the skull was cleaned, the head was fixed in a custom-made acrylic glass frame. The top of the skull was pushed against the acrylic frame as close as possible. Four stainless-steel screw bars (6 mm diameter, 10 cm length) held the head steady on each side. Once the head was positioned, the positions of the 36 penetration holes were marked by an ink-filled needle through the pre-made matrix of holes of the plexiglass back panel. The frame was removed, and holes were drilled (1.2 mm diameter) and rinsed by physiologic saline. The frame was placed

back to its original position, and the head was repositioned by the screw bars. Four or seven pairs of stimulation electrodes (Ag/AgCl EEG electrodes, 10 mm diameter, Ambu) were placed between the rubber rings and the skull surface with conductive paste (Ten20). Custom-made multiple-site electrodes were prepared as follows: three to seven holes were drilled on the outer surface of a translucent polyimide tube (775 µm outside diameter) 1 cm from each other. Three to seven 127-µm diameter, polyurethane-insulated, copper-nickel wires were threaded into the polyimide tube through these holes. The wires were secured by a drop of cyano-acrylic glue at the side-holes of the polyimide tube and the other end of it was soldered to a connector socket. The tubes were backfilled with epoxy glue to increase stiffness. Once the epoxy dried, the wires were cut back at the surface of the polyimide tube, and the tip of the tube was sharpened (Fig. 12a). Impedances of the contact sites varied between 50 and 300 kΩ at 1 kHz. Electrodes were inserted into the brain through the previously drilled skull holes and the matching plexiglass matrix while rotating continuously, to preserve parallel alignment (Fig. 12b, c).

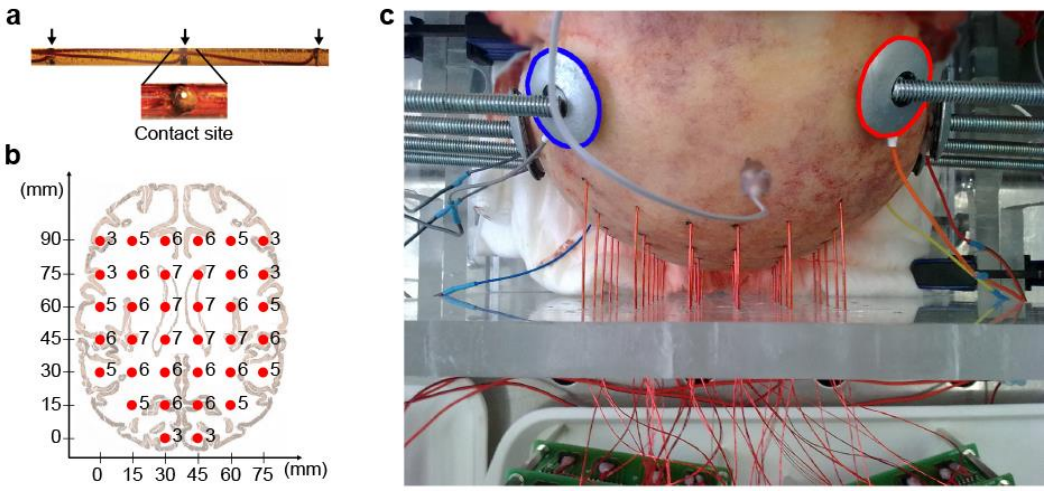

Figure 12. Photographs of cadaver recording arrangements
a Photomicrograph of the custom-made multicontact electrodes used in the cadaver experiments. **b** Stereotaxic coordinates of the electrode shanks. Numbers denote the number of recording sites for each electrode shank. Electrode tips (and adjacent sites) were positioned at the same depth to sample distinct horizontal planes. The depth coverage of our electrodes was 3–7 cm (depending on the number of contact sites). **c** Photograph of the skull with drilled holes and inserted electrodes. A needle electrode in the sagittal plane on the forehead served as reference.

A needle was inserted through the skull above the prefrontal cortex and served as reference electrode. Physiologic saline solution (2–5 ml) was injected through the same hole to refill the cerebrospinal fluid lost during the drilling procedure. Recording

electrodes made a watertight seal in the skull holes, thus further leakage was not significant. The chest wall was used as grounding. Subcutaneous (electrodes placed on the skull surface) alternating current stimulation was performed using stimulation signals generated by an STG 4008–16 mA (Multi Channel Systems). The stimulating electrodes of the two sides were paired using different parallel or diagonal arrangements. Sinusoid stimuli with varying intensities (1, 2, 3, 4, 5, and 6 V) at 10 Hz and varying frequencies (5, 20, 50, 100, 200, 500, 1000, and 2000 Hz) at 5 V were used for at least 500 cycles, each. To mimic the effect of increasing electrode sizes, multiple stimulating electrodes were coupled together. The recorded signals ($n = 198$ channels) were amplified (10× gain) and stored after digitization at 20 kHz sampling rate per channel by a custom-designed recoding system based on the RHD2000 Evaluation System (for AC coupled recordings, 0.1–6 kHz bandwidth, Intan Technologies). To measure the electric field, 500 sinus cycles were averaged for each stimulation condition and then peak-to-peak amplitude was measured for each channel. The first spatial derivative of these voltage signals was calculated.

Measuring the shunting effect of the skin and skull in human cadavers

Instead of retracting the skin, four or six 5-mm long incisions (15 mm apart from each other) were made in the coronal plane, connecting one mastoid with the other. Then 1.3 mm diameter holes were drilled. Stimulation electrodes (n = 4, Ag/AgCl, Ambu) were attached to the skin by conductive paste (Ten20). Four or six custom-made 7 contact site recording electrodes were inserted into the brain, transcutaneous AC stimulation was performed, as described above. The recorded signals (n = 28 or 42 channels) were amplified (10× gain) and stored after digitization at 15 kHz sampling rate per channel (RHD2000 Evaluation System, Intan Technologies). After the skin measurements, the skin incisions were carefully connected, and the scalp was removed while the recording electrodes were kept in place. The stimulating electrodes were attached to the skull surface and the same stimulation protocol was applied. In separate experiments, to compare the effect of subcutaneous stimulation to intracranial stimulations, in some cases additional stimulating electrodes were placed intracranially, in between the subcutaneous electrodes as follows: the additional skull holes were drilled with incrementally increasing (2, 4 and 8 mm) drill-bit sizes, and externally threaded, hollow plastic dowels (15 mm long, 8 mm diameter) were introduced in the holes to form an electrical isolation toward the skull. Sponge electrodes with the encapsulated Ag/AgCl plates, soaked in

physiologic saline, were glued to the tip of screws, and introduced into the plastic dowels to touch the surface of the brain.

Registering the anthropometric data of the cadavers

At the end of the measurements, the cranium was opened with an oscillating saw in the line of the stimulating electrodes. After removing the skull cap, the brain was also removed. Anthropometric data of the skull was measured (circumference, sagittal, horizontal, vertical distance, and skull thickness below the stimulating electrodes) (Table 1). After the brain was examined by the pathologist, a 5-g piece of the occipital lobe was removed to measure the water content of the brain tissue by desiccation. As reference, hydration value of living tissue was taken from reference.

#	Age	Sex	Weight (kg)	Post-mortem age (day)	Brain water (%)	Brain weight (g)	Skull circumference (cm)	Skull thickness (mm)								Cause of death
								L1	L2	L3	L4		R1	R2	R3	R4	
1/18	94	M	43	3	80.37	1235	50.7	6	7	5	6		5	5	4	6	Bronchopneumonia
1/19	86	M	59	6	81.56	1360	52.3	4	4	4	3		3	5	4	4	Bronchopneumonia
1/20	87	F	67	8	78.29	1115	49	6	6	5	4		5	4	4	5	Klatschkin-tumor
1/21	92	F	54	7	81.01	1075	49.8	8	6	5	5		9	4	6	4	Heart failure
2/2	94	M	58	5	82.57	1105	47.8	6	5	4	5		6	6	4	4	Heart failure
2/3	65	M	57	5	82.94	1025	-	-	-	-	-		-	-	-	-	Acute myeloid leukemia
2/4	67	M	53	7	80.49	1340	50.8	4	4	4	5		3	5	4	6	Lung adenocarcinoma
3/2	82	F	51	4	78.95	1200	49.5	4	3	5	6		4	4	5	6	Pancreas adenocarcinoma
3/3	76	F	78	7	83.15	1210	52	9	6	4	6		9	5	5	6	Pulmonary embolism
3/4	94	F	45	3	83.87	1105	49.2	10	4	4	6		3	5	5	3	Bronchopneumonia
3/5	88	F	62	3	81.73	1220	50.5	10	5	6	4		3	4	4	5	Bronchopneumonia
3/6	69	F	43	3	86.36	1225	-	-	-	-	-		-	-	-	-	Bronchopneumonia
3/s1	80	F	120	6	83.33	1210	49.6	6	5	3	4						Invasive ductal adenocarcinoma of the breast
3/s2	59	F	78	7	-	1120	50.4	6	4	4	5						Heart failure
4/1	82	M	-	3	88.77	1455	54	-	5	-	-		-	4	-	-	Hypovolemic shock
4/2	73	M	-	7	81.54	1255	51.8	-	5	-	-		-	5	-	-	Bronchopneumonia
4/3	80	M	-	2	87	1480	54.2	-	4	-	-		-	4	-	-	Acute myocardial infarction
Mean	**80.5**		**62**	**5.1**	**82.6**	**1219.7**	**50.8**	**6.6**	**4.9**	**4.4**	**4.9**		**5.0**	**4.6**	**4.5**	**4.9**	

Table 1. Anthropometric data of the cadavers
L1-4 and R1-4 refer to the 4 location of stimulating electrodes on the left and right sides, respectively. L1 and R1 denote the two most frontal locations.

ISP stimulation on human subjects

Human transcutaneous ISP stimulation and EEG recording were performed on healthy subjects (all males, age = 21–66 years). Subjects with short hair were preferably selected, thus including only males was incidental. All subjects gave their informed consent to the measurements. Each subject served as his own control.

Before stimulation, each subject was briefly exposed to a few seconds of 1 Hz constant current stimulation with increasing intensities (1, 2, 4, and 8 mA) to familiarize them with the expectable subjective experience, and to test if any adverse effects are present. The intensity was increased to the next level only if the previous intensity was reported as being well tolerable. In addition to the well documented tingling, burning feeling of the skin and perception of phosphenes, stimulus intensities above 4.5 mA stimulation induced feeling of horizontal head-movements and horizontal oscillation of the visual and auditory fields at the frequency of the stimulation. All subjective effects were stronger at the beginning of the stimulation and attenuated during the course of stimulation. One of 19 subjects in the ramp stimulation experiments requested to terminate stimulation because of feeling dizzy. In one of them, the instability of the electrodes was only discovered after the experiments and the results from this subject could not be analyzed due to excessive artifacts.

EEG recording during ISP stimulation

EEG scalp recordings were performed by a V-Amp amplifier and ActiCap BP active electrodes (Brain Products). Impedances were measured online and adjusted to remain below 20 kΩ by applying electrode gel. Electrodes were placed according to the International 10/20 electrode scheme (P3 and P4 locations). The broad dynamic range of the active electrodes, and their buffering capacity allowed the low-noise transmission of EEG signals and stimulus artifacts without on-head amplification. To prevent the saturation of the amplifier, the output range of the active electrodes was matched to the input range of the EEG amplifier through custom-made voltage dividers.

Stimulating sponge electrodes for ISP were prepared from a 2 × 3 × 1.5 cm sponge glued to a 2 × 3 cm copper mesh and glued to a rubber washer with the sponges inside, keeping approximately 2.5 cm distance between sponges. The rubber washer with the 12 electrodes was soaked in 0.9% saline solution and tightened gently around the head. Conductivity was further improved by putting electrode gel (SuperVisc, EasyCap)

between the wet sponges and the skin. For abdominal ISP stimulation, the same sponge electrodes were placed around the trunk.

The ISP stimulation consisted of 6 x 10 µs pulses repeated at 16.66 kHz (~16% duty cycle on each electrode). The amplitude of the pulses was modulated by a 1-Hz sine wave, linearly ramping up from zero to maximum in 6 seconds, then ramping down to zero in 6 seconds (Fig. 13)

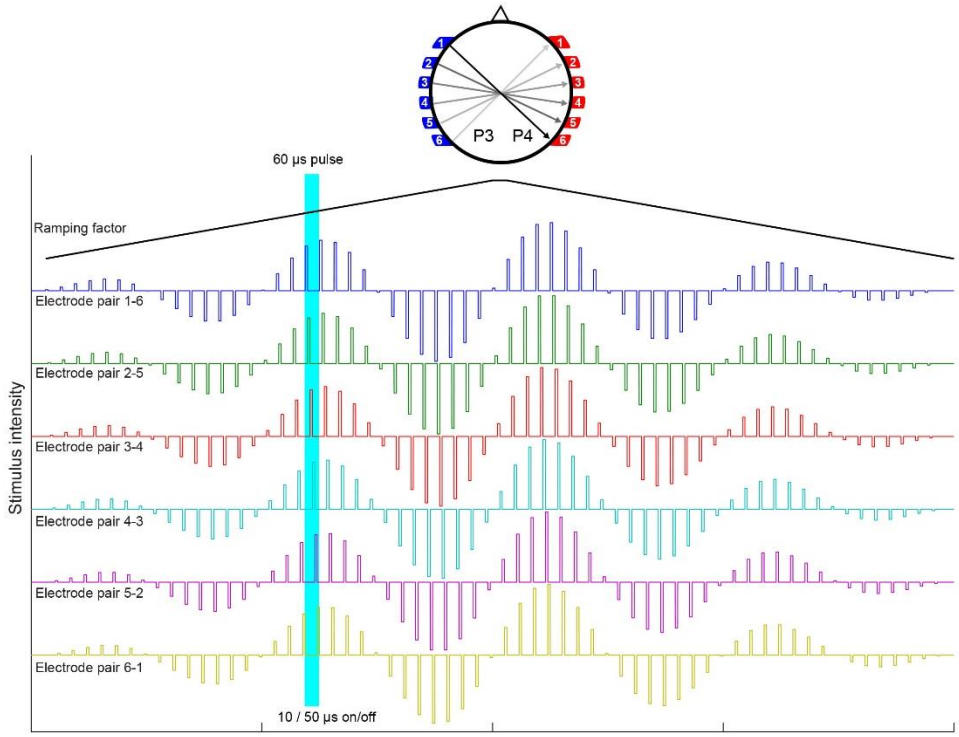

Figure 13. Illustration of human ISP protocol.
Upper part shows the position of the recording (P3 and P4) and stimulating electrodes in human measurements. Lower part shows a single trial. The amplitude of the pulses was modulated by a 1-Hz sine wave, linearly ramping up from zero to maximum in 6 seconds, then ramping down to zero in 6 seconds. The duration of the 10 µs pulses is shown disproportionally longer for better visibility.

ISP stimulation induced artefact removal

To remove the stimulus artifact (Fig. 14a), we subtracted the triggered moving average ($t = 10$ epochs) from the signal, followed by triple-sweeps of 100th order zero phase-lag high-pass finite impulse response filter ($f = 2$ Hz) in MATLAB. Then we filtered the artifact-free signal (Fig. 14b) in the alpha band (8-12 Hz) with a zero phase-lag fourth-order Butterworth filter (Fig. 14c, d). Instantaneous alpha amplitudes were determined by calculating the magnitude of the Hilbert-transformed filtered signal and binned based on the corresponding ISP amplitude and phase. Binned values were averaged across epochs.

To estimate the amplitude of the remaining electrical noise time locked to the epochs, signal was first averaged across epochs, and then Hilbert transformed. This approach preserved time-locked features. For frequency domain analyses, spectral amplitudes were calculated using fast-Fourier transformation, and smoothed using a moving average filter (width = 2 Hz). 120 - 140 Hz was chosen as a control frequency band, as this range does not represent measurable physiological oscillatory signals on the scalp but would still mirror the presence of broadband electrical artifacts. For time-resolved spectral analysis, spectra were calculated using a multitaper fast Fourier transform on 1-s long consecutive segments. Spectra were whitened by multiplying each frequency by the frequency value (1/f method).

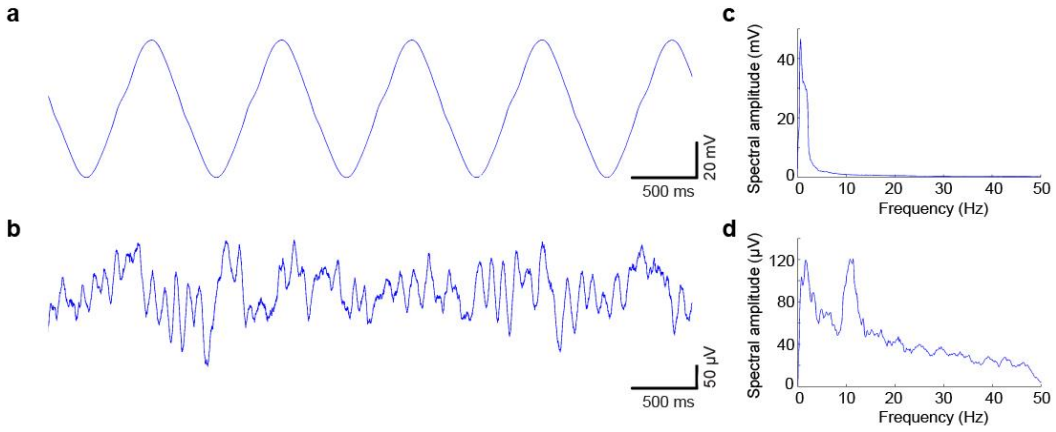

Figure 14. EEG artefact removal.
a, b Example trace showing EEG recording before (**a**) and after artefact removal (**b**).
c, **d** Panels show the corresponding power spectra of EEG traces shown on the left.
Stimulus intensity is 7 mA.

Frequency-amplitude and phase-amplitude analysis of EEG

Antonio Fernandez-Ruiz performed this analysis.

We employed two complementary analyses to assess the modulation of EEG amplitude by the phase of the sinusoidal ISP stimulation current. Analyses were performed on 1-min-long consecutive epochs, and the epoch results were pooled. First, we applied the complex wavelet transform using Morlet mother wavelets to calculate the amplitude and phase for a wide range of EEG frequencies. Wavelet amplitudes were calculated from 1 to 30 Hz at 59 levels from the artifact-free EEG and wavelet phase for 21 levels from 0.5 to 5 Hz at 15 levels from either the original EEG or a synthetic signal constructed from the stimulation pulses. Phase–amplitude cross-frequency coupling was quantified using a modulation index (MI)[113]. To quantify frequency–amplitude modulation, 2-D

comodulograms were constructed with the MI values for every phase–amplitude frequency pair and the maximal MI in the band of interest was detected[114]. For phase–amplitude modulation, phase time-series were binned into phase intervals and the mean wavelet amplitude was calculated for each of them and *z*-scored. Phase time-series were binned into phase intervals and the mean wavelet amplitude was calculated for each of them[114].

For a complementary phase–amplitude analysis performed on the time domain, the estimated peak-to-peak amplitude values of the individual alpha waves were binned based on the actual stimulus phase, and alpha amplitude values during the stimulus peak and trough bins (45, 90, 135, 225, 270, 315°) were compared to the alpha amplitude values present at the transitional phase (0° and 180°) bins using a *t*-test.

ISP stimulation in rats

Modeling of ISP stimulation induced electric fields

We used a leaky-integrate and fire neuron model to visualize the principle of ISP stimulation. Extracellular electric fields were derived from in vivo tACS measurements using 1 kHz sinusoid stimuli using epidural stimulation with screw electrodes. The directionless electric field intensities (35 V/m peak intensity) at each point were converted to intracellularly injected current values by multiplying with an arbitrary factor (4.5 nA/mV/mm) to mimic demonstrative transmembrane currents. A dimensionless leaky-integrate and fire neuron model was established in Matlab[94]. Parameters were set as the following: temporal constant of the membrane = 10 ms; resting membrane potential = −70 mV; membrane resistance = 1 MΩ; spiking threshold = −54 mV; spike peak potential = 20 mV; repolarization level = −80 mV. Extracellular electric field duration = 0.5 ms. The effects of three different magnitude current injections on the firing rate were demonstrated by the leaky-integrate and fire neuron model is illustrated in Fig. 11a.

In vivo, extracellular recordings during ISP stimulation

Two custom-designed stimulation strips were 3-D printed and glued bilaterally on the surfaces of the temporal bones of the rats by cyano-acrylic glue. Each of the two symmetric strips (width 13 mm, height 3.3 mm, and wall thickness 0.7 mm) consisted of five individual pockets which were spaced by 3.7, 2.2, 2.2, and 3.7 mm (Fig. 15a), and their medial surfaces were resembling the temporal bone curvature of a magnetic resonance imaging (MRI) data-based 3D model of a rat skull. The middle pockets were

positioned at 5.16 mm posterior from bregma. The pockets were filled with conductive paste through filling holes left open at the top (Super Visc, Brain Products) and then sealed with silicon. Craniotomies were drilled (2.2 mm diameter) and two silicon probes (Buzsaki32-H32; NeuroNexus) were implanted at 5.16 mm posterior from bregma and 4 mm lateral of the midline, in the CA1 region of the hippocampus (Fig. 15a). The hole around the probes was filled with non-conductive silicone (Dow Corning®). Proper locations of the electrodes were confirmed by the characteristic electrophysiological landmarks of the broadband signal at the pyramidal layer of CA1. ISP stimulation was performed in a voltage-controlled mode using phototransistor-based custom-made electronics. Each trial consisted of 3 x 2.5 µs pulses repeated at 133 kHz (100% duty cycle) for 500 ms and followed by 1 s pause (Fig. 15b).

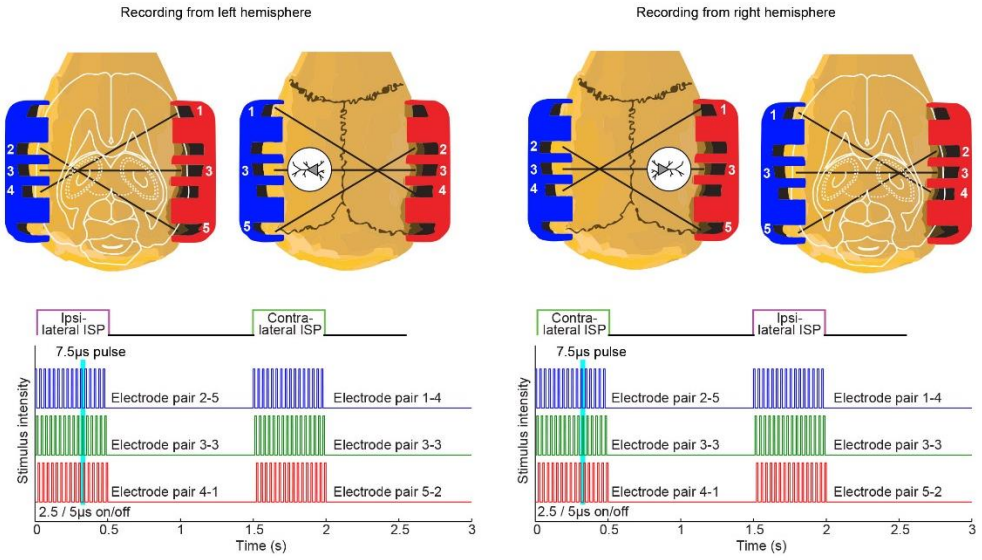

Figure 15. Illustration of rat ISP protocol.
a Neuronal activity was recorded from both hemispheres simultaneously (white circles corresponds to the location of craniotomies). The ISP was alternatingly focused to left or right hemisphere. **b** schematics of the stimulation sequence for two consecutive trials. The duration of the 2.5 µs pulses is shown disproportionally longer for better visibility.

Comparing the effect of DC and ISP stimulation

To compare the effects of ISP and DC stimulation in rats, the same surgery procedure was applied but the stimulation was performed in current-controlled mode (stimulus intensity 200 µA) using a high-speed analog switch-based circuits. The recorded signals ($n = 64$ channels) were amplified (400× gain) and stored after digitization at 20 kHz sampling rate per channel (KJE-1001, Amplipex). We repeated the same measurements on one awake, freely moving animal.

The recorded data were analyzed by custom-written scripts in MATLAB (MathWorks). Neuronal spikes were detected from the digitally high-pass filtered signal (1–3 kHz) by Spikedetekt2 (https://github.com/klusta-team/spikedetekt2). Detected spikes were automatically sorted using KlustaKwik2[115], followed by manual adjustment of the clusters using KlustaViewa software[116] to get well-isolated single units (multi-unit and noise clusters were discarded).

Acknowledgments

First and foremost, I thank my advisor, Dr. Antal Berényi for giving me the opportunity to do the PhD in his lab. I am extremely grateful to him for introducing me into the world of science as a third-year medical student. He always gave me the freedom to explore new ideas, attend to and present at conferences and workshops. These experiences have taught me how to be a better researcher while developing my overall professional skillset. I sincerely thank him for his continuous support and guidance.

I express my gratitude to the Doctoral School of Theoretical Medicine at the University of Szeged lead by Professor Gábor Jancsó for accepting me in their PhD Program; and to Professor Gyula Sáry for allowing me to work in the Department of Physiology. I thank to everyone in the Department of Physiology for welcoming me and being supportive whenever I needed.

I could not carry out the cadaver experiments without the initial help of Kitti and Peti who turned the impossible into possible in the autopsy room. I thank to Tomi for his help with experiments and to Professor Béla Iványi for his continuous support.

I am thankful to Antonio and Aza. They explained Maxwell's equations to me many times throughout my PhD but more importantly they showed me the skill of critical thinking and introduced the 'Science is a lifestyle' philosophy. I also thank to Gábor for the many hours of constructive discussions during the 'Coffee break with Gábor in the library', and for the fights at the football field. Lastly but not the least, I am thankful to Ancsa, Bereniké, Árpi, Yuichi, Gergő and Mari for helping me with everything during the course of my time in the Berényi lab.

Professor György Buzsáki has been an exceptional role model. His work in the field of neuroscience have inspired my research in many ways. His guidance and encouragement have been instrumental to my graduate career.

Finally, my deepest gratitude and most heartfelt thanks to my family – Csilla, Ildi and Balázs – for their constant love and support. Thank you for always lending a listening ear and a helping hand. I thank my Mom, who have taught me how to work hard for something and to never ever, give up. Finally, and most importantly, I thank my wife, Claudia. She has supported me every possible way throughout my PhD. Her never-ending patience allowed me to work late nights and weekends and she was always available at 11 p.m. when I needed someone to bring me home from the lab. I cannot thank her enough for her support.

References

1. Kellaway, P. The part played by electric fish in the early history of bioelectricity and electrotherapy. *Bull. Hist. Med.* **20**, (1946).

2. Rudorfer, M. V., Henry, M. E. & Sackeim, H. A. Electroconvulsive Therapy. in *Psychiatry* (eds. Tasman, A., Kay, J. & A., J.) 1865–1901 (wiley, 2003).

3. Benabid, A. L. *et al.* Long-term suppression of tremor by chronic stimulation of the ventral intermediate thalamic nucleus. *Lancet (London, England)* **337**, 403–6 (1991).

4. Kringelbach, M. L., Jenkinson, N., Owen, S. L. F. & Aziz, T. Z. Translational principles of deep brain stimulation. *Nat. Rev. Neurosci.* **8**, 623–635 (2007).

5. Nitsche, M. A. & Paulus, W. Excitability changes induced in the human motor cortex by weak transcranial direct current stimulation. *J. Physiol.* **527 Pt 3**, 633–9 (2000).

6. Brunoni, A. R., Nitsche, M. & Loo, C. *Transcranial Direct Current Stimulation in Neuropsychiatric Disorders*. (Springer, 2016). doi:10.1007/978-3-319-33967-2

7. Anastassiou, C. A., Montgomery, S. M., Barahona, M., Buzsaki, G. & Koch, C. The Effect of Spatially Inhomogeneous Extracellular Electric Fields on Neurons. *J. Neurosci.* **30**, 1925–1936 (2010).

8. Anastassiou, C. a, Perin, R., Markram, H. & Koch, C. Ephaptic coupling of cortical neurons. *Nat. Neurosci.* **14**, 217–23 (2011).

9. Jefferys, J. G. R. Nonsynaptic Modulation of Neuronal Activity in the Brain : Electric Currents and Extracellular Ions. *Physiol. Rev.* **75**, 689–723 (1995).

10. Buzsáki, G. & Wang, X.-J. Mechanisms of Gamma Oscillations. *Annu. Rev. Neurosci.* **35**, 203–225 (2012).

11. Paulus, W. Transcranial electrical stimulation (tES - tDCS; tRNS, tACS) methods. *Neuropsychol. Rehabil.* **21**, 602–617 (2011).

12. Gabriel, S., Lau, R. W. & Gabriel, C. The dielectric properties of biological tissues: II. Measurements in the frequency range 10 Hz to 20 GHz. *Phys. Med. Biol.* **41**, 2251–69 (1996).

13. Gabriel, C., Gabriel, S. & Corthout, E. The dielectric properties of biological tissues: I. Literature survey. *Phys. Med. Biol.* **41**, 2231–49 (1996).

14. Yamamoto, T. & Yamamoto, Y. Electrical properties of the epidermal stratum corneum. *Med. Biol. Eng.* **14**, 151–158 (1976).

15. Truong, D. Q., Magerowski, G., Blackburn, G. L., Bikson, M. & Alonso-Alonso, M. Computational modeling of transcranial direct current stimulation (tDCS) in obesity: Impact of head fat and dose guidelines. *NeuroImage Clin.* **2**, 759–766

(2013).

16. Gielen, F. L. *et al.* Model of electrical conductivity of skeletal muscle based on tissue structure. *Med. Biol. Eng. Comput.* **24**, 34–40 (1986).

17. Shahid, S., Wen, P. & Ahfock, T. Effect of fat and muscle tissue conductivity on cortical currents - A tDCS study. in *2011 IEEE/ICME International Conference on Complex Medical Engineering, CME 2011* 211–215 (2011). doi:10.1109/ICCME.2011.5876735

18. Opitz, A., Paulus, W., Will, S., Antunes, A. & Thielscher, A. Determinants of the electric field during transcranial direct current stimulation. *Neuroimage* **109**, 140–150 (2015).

19. Logothetis, N. K., Kayser, C. & Oeltermann, A. In Vivo Measurement of Cortical Impedance Spectrum in Monkeys: Implications for Signal Propagation. *Neuron* **55**, 809–823 (2007).

20. Nicholson, P. W. Specific impedance of cerebral white matter. *Exp. Neurol.* **13**, 386–401 (1965).

21. Bindman, L. J., Lippold, O. C. J. & Redfearn, J. W. T. The action of brief polarizing currents on the cerebral cortex of the rat (1) during current flow and (2) in the production of long-lasting after-effects. *J. Physiol.* **172**, 369–382 (1964).

22. Creutzfeldt, O. D., Fromm, G. H. & Kapp, H. Influence of transcortical d-c currents on cortical neuronal activity. *Exp. Neurol.* **5**, 436–452 (1962).

23. Purpura, D. P. & McMurtry, J. G. Intracellular Activities and Evoked Potential Changes During of motor cortex. *Neurophysiol* **28**, 166–185 (1965).

24. Moliadze, V., Antal, A. & Paulus, W. Electrode-distance dependent after-effects of transcranial direct and random noise stimulation with extracephalic reference electrodes. *Clin. Neurophysiol.* **121**, 2165–71 (2010).

25. Bikson, M., Datta, A., Rahman, A. & Scaturro, J. Electrode montages for tDCS and weak transcranial electrical stimulation: role of 'return' electrode's position and size. *Clin. Neurophysiol.* **121**, 1976–8 (2010).

26. Rahman, A. *et al.* Cellular effects of acute direct current stimulation: somatic and synaptic terminal effects. *J. Physiol.* **591**, 2563–78 (2013).

27. Chan, C. Y., Hounsgaard, J. & Nicholson, C. Effects of electric fields on transmembrane potential and excitability of turtle cerebellar purkinje cells in vitro. *J. Physiol* **402**, 751–771 (1988).

28. Bikson, M. *et al.* Effects of uniform extracellular DC electric fields on excitability in rat hippocampal slices in vitro. *J. Physiol.* **557**, 175–90 (2004).

29. Joucla, S. & Yvert, B. The mirror estimate: an intuitive predictor of membrane polarization during extracellular stimulation. *Biophys. J.* **96**, 3495–508 (2009).

30. Datta, A., Bikson, M. & Fregni, F. Transcranial direct current stimulation in patients with skull defects and skull plates: high-resolution computational FEM study of factors altering cortical current flow. *Neuroimage* **52**, 1268–78 (2010).

31. Cohen Kadosh, R. *The Stimulated Brain*. (Elsevier, 2014). doi:10.1017/CBO9781107415324.004

32. Brunoni, A. R. *et al.* The Escitalopram versus Electric Current Therapy for Treating Depression Clinical Study (ELECT-TDCS): rationale and study design of a non-inferiority, triple-arm, placebo-controlled clinical trial. *Sao Paulo Med. J.* **133**, 252–263 (2015).

33. Jackson, M. P. *et al.* Safety parameter considerations of anodal transcranial Direct Current Stimulation in rats. *Brain. Behav. Immun.* **64**, 152–161 (2017).

34. Vöröslakos, M. *et al.* Direct effects of transcranial electric stimulation on brain circuits in rats and humans. *Nat. Commun.* **9**, 483 (2018).

35. Reato, D., Rahman, A., Bikson, M. & Parra, L. C. Low-Intensity Electrical Stimulation Affects Network Dynamics by Modulating Population Rate and Spike Timing. *J. Neurosci.* **30**, 15067–15079 (2010).

36. Ozen, S. *et al.* Transcranial electric stimulation entrains cortical neuronal pupulations in rats. *J. Neurosci* **30**, 11476–11485 (2010).

37. Fertonani, A., Ferrari, C. & Miniussi, C. What do you feel if I apply transcranial electric stimulation? Safety, sensations and secondary induced effects. *Clin. Neurophysiol.* **126**, 2181–2188 (2015).

38. Poreisz, C., Boros, K., Antal, A. & Paulus, W. Safety aspects of transcranial direct current stimulation concerning healthy subjects and patients. *Brain Res. Bull.* **72**, 208–214 (2007).

39. Datta, A. *et al.* Gyri –precise head model of transcranial DC stimulation: Improved spatial focality using a ring electrode versus conventional rectangular pad. *Brain Stimul.* **2**, 201–207 (2009).

40. Lafon, B. *et al.* Low frequency transcranial electrical stimulation does not entrain sleep rhythms measured by human intracranial recordings. *Nat. Commun.* **8**, 1–14 (2017).

41. Huang, Y. *et al.* Measurements and models of electric fields in the in vivo human brain during transcranial electric stimulation. *Elife* **6**, 1–26 (2017).

42. Opitz, A., Falchier, A., Yan, C., Yeagle, E. & Linn, G. Spatiotemporal structure of intracranial electric fields induced by transcranial electric stimulation in human and nonhuman primates. *Sci. Rep.* **6**, 1–11 (2016).

43. Cogiamanian, F., Marceglia, S., Ardolino, G., Barbieri, S. & Priori, A. Improved isometric force endurance after transcranial direct current stimulation over the human motor cortical areas. *Eur. J. Neurosci.* **26**, 242–249 (2007).

44. Datta, A., Elwassif, M., Battaglia, F. & Bikson, M. Transcranial current stimulation focality using disc and ring electrode configurations: FEM analysis. *J. Neural Eng.* **5**, 163–174 (2008).

45. Liebetanz, D. *et al.* Safety limits of cathodal transcranial direct current stimulation in rats. *Clin. Neurophysiol.* **120**, 1161–1167 (2009).

46. Dockery, C. A., Liebetanz, D., Birbaumer, N., Malinowska, M. & Wesierska, M. J. Cumulative benefits of frontal transcranial direct current stimulation on visuospatial working memory training and skill learning in rats. *Neurobiol. Learn. Mem.* **96**, 452–460 (2011).

47. Kozák, G. & Berényi, A. Sustained efficacy of closed loop electrical stimulation for long-term treatment of absence epilepsy in rats. *Sci. Rep.* **7**, 1–10 (2017).

48. Berenyi, A., Belluscio, M., Mao, D. & Buzsaki, G. Closed-Loop Control of Epilepsy by Transcranial Electrical Stimulation. *Science (80-.).* **337**, 735–737 (2012).

49. Ozen, S. Biasing Neural Activity: Entraiment of Cortical Neurons by Applied Electric Fields. *Thesis* (2010).

50. Laste, G. *et al.* After-effects of consecutive sessions of transcranial direct current stimulation (tDCS) in a rat model of chronic inflammation. *Exp. Brain Res.* **221**, 75–83 (2012).

51. Nitsche, M. A. *et al.* Shaping the effects of transcranial direct current stimulation of the human motor cortex. *J. neurophysiol* **97**, 3109–3117 (2007).

52. Turi, Z. *et al.* When size matters: Large electrodes induce greater stimulation-related cutaneous discomfort than smaller electrodes at equivalent current density. *Brain Stimul.* **7**, 460–467 (2014).

53. Chan, C. Y. & Nicholson, C. Modulatoin by Applied Electric Fields of Purkinje and Stellate Cell Activity in the Isolated Turtle Cerebellum. *J. Physiol* **371**, 89–114 (1986).

54. Deans, J. K., Powell, A. D. & Jefferys, J. G. R. Sensitivity of coherent oscillations in rat hippocampus to AC electric fields. *J. Physiol.* **583**, 555–565 (2007).

55. Ali, M. M., Sellers, K. K. & Fröhlich, F. Transcranial alternating current stimulation modulates large-scale cortical network activity by network resonance. *J. Neurosci.* **33**, 11262–75 (2013).

56. Binder, S. *et al.* Transcranial slow oscillation stimulation during sleep enhances memory consolidation in rats. *Brain Stimul.* **7**, 508–515 (2014).

57. Binder, S., Rawohl, J., Born, J. & Marshall, L. Transcranial slow oscillation stimulation during NREM sleep enhances acquisition of the radial maze task and modulates cortical network activity in rats. *Front. Behav. Neurosci.* **7**, 1–10 (2014).

58. Greenberg, A., Karimi, J., Dickson, C. T. & Mohajerani, M. H. New waves : Rhythmic electrical field stimulation systematically alters spontaneous slow dynamics across mouse neocortex. *Neuroimage* **174**, 328–339 (2018).

59. Greenberg, A., Whitten, T. A. & Dickson, C. T. Stimulating forebrain communications : Slow sinusoidal electric fields over frontal cortices dynamically modulate hippocampal activity and cortico-hippocampal interplay during slow-wave states. *Neuroimage* **133**, 189–206 (2016).

60. Zaehle, T., Rach, S. & Herrmann, C. S. Transcranial alternating current stimulation enhances individual alpha activity in human EEG. *PLoS One* **5**, e13766 (2010).

61. Antal, A. *et al.* Comparatively weak after-effects of transcranial alternating current stimulation (tACS) on cortical excitability in humans. *Brain Stimul.* **1**, 97–105 (2008).

62. Helfrich, R. F. *et al.* Entrainment of brain oscillations by transcranial alternating current stimulation. *Curr. Biol.* **24**, 333–339 (2014).

63. Neuling, T. *et al.* Friends, not foes: Magnetoencephalography as a tool to uncover brain dynamics during transcranial alternating current stimulation. *Neuroimage* **118**, 406–413 (2015).

64. Noury, N., Hipp, J. F. & Siegel, M. Physiological processes non-linearly affect electrophysiological recordings during transcranial electric stimulation. *Neuroimage* **140**, 99–109 (2016).

65. Bikson, M. *et al.* Safety of transcranial Direct Current Stimulation: Evidence Based Update 2016. *Brain Stimul.* **9**, 641–661 (2017).

66. Bikson, M., Datta, A. & Elwassif, M. Establishing safety limits for transcranial direct current stimulation. *Clin. Neurophysiol.* **120**, 1033–4 (2009).

67. Jackson, M. P. *et al.* Animal models of transcranial direct current stimulation: Methods and mechanisms. *Clin. Neurophysiol.* **127**, 3425–3454 (2016).

68. Palm, U. *et al.* Skin lesions after treatment with transcranial direct current stimulation (tDCS). *Brain Stimul.* **1**, 386–387 (2008).

69. Brunoni, A. R. *et al.* A systematic review on reporting and assessment of adverse effects associated with transcranial direct current stimulation. *Int. J. Neuropsychopharmacol.* **14**, 1133–1145 (2011).

70. Bikson, M., Bestmann, S. & Edwards, D. Neuroscience: transcranial devices are not playthings. *Nature* **501**, 167 (2013).

71. Wexler, A. The practices of do-it-yourself brain stimulation: Implications for ethical considerations and regulatory proposals. *J. Med. Ethics* **42**, 211–215 (2016).

72. Squire, L. R. *Fundamental neuroscience*. (Academic Press, 2012).

73. Buzsáki, G. *Rhythms of the Brain*. (Oxford University Press, 2006). doi:10.1093/acprof:oso/9780195301069.001.0001

74. Bindman, L. J., Lippold, O. C. J. & Redfearn, J. W. T. Long-lasting changes in the level of the electrical activity of the cerebral cortex produced by polarizing currents. *Nature* **196**, 584–585 (1962).

75. Radman, T., Su, Y., An, J. H., Parra, L. C. & Bikson, M. Spike timing amplifies the effect of electric fields on neurons: implications for endogenous field effects. *J. Neurosci.* **27**, 3030–6 (2007).

76. Henze, D. A. & Buzsáki, G. Action potential threshold of hippocampal pyramidal cells in vivo is increased by recent spiking activity. *Neuroscience* **105**, 121–30 (2001).

77. Radman, T., Ramos, R. L., Brumberg, J. C. & Bikson, M. Role of cortical cell type and morphology in subthreshold and suprathreshold uniform electric field stimulation in vitro. *Brain Stimul.* **2**, 215–28, 228.e1–3 (2009).

78. Woods, A. J. *et al.* A technical guide to tDCS, and related non-invasive brain stimulation tools. *Clin. Neurophysiol.* **127**, 1031–1048 (2016).

79. Marshall, L. & Binder, S. Contribution of transcranial oscillatory stimulation to research on neural networks: an emphasis on hippocampo-neocortical rhythms. *Front. Hum. Neurosci.* **7**, 614 (2013).

80. Herrmann, C. S., Rach, S., Neuling, T. & Strüber, D. Transcranial alternating current stimulation : a review of the underlying mechanisms and modulation of cognitive processes. *Front. Hum. Neurosci.* **7**, 1–13 (2013).

81. Fröhlich, F. & McCormick, D. A. Endogenous electric fields may guide neocortical network activity. *Neuron* **67**, 129–143 (2010).

82. McDonnell, M. D. & Abbott, D. What Is Stochastic Resonance? Definitions, Misconceptions, Debates, and Its Relevance to Biology. *PLoS Comput. Biol.* **5**, e1000348 (2009).

83. Thut, G., Schyns, P. G. & Gross, J. Entrainment of perceptually relevant brain oscillations by non-invasive rhythmic stimulation of the human brain. *Frontiers in Psychology* **2**, 170 (2011).

84. Liu, A. *et al.* Immediate neurophysiological effects of transcranial electrical stimulation. *Nat. Commun.* **9**, 5092 (2018).

85. Greenberg, A. & Dickson, C. T. NeuroImage Spontaneous and electrically modulated spatiotemporal dynamics of the neocortical slow oscillation and associated local fast activity. *Neuroimage* **83**, 782–794 (2013).

86. Grossman, N. *et al.* Noninvasive Deep Brain Stimulation via Temporally Interfering Electric Fields. *Cell* **169**, 1029-1041.e16 (2017).

87. Noury, N. & Siegel, M. Analyzing EEG and MEG signals recorded during tES, a

reply. *Neuroimage* **167**, 53–61 (2018).

88. Wagner, T. *et al.* Transcranial direct current stimulation: A computer-based human model study. *Neuroimage* **35**, 1113–1124 (2007).

89. Wagner, T. a, Zahn, M., Grodzinsky, A. J. & Pascual-Leone, A. Three-dimensional head model simulation of transcranial magnetic stimulation. *IEEE Trans. Biomed. Eng.* **51**, 1586–1598 (2004).

90. Faria, P., Hallett, M. & Miranda, P. C. A finite element analysis of the effect of electrode area and inter-electrode distance on the spatial distribution of the current density in tDCS. *J. Neural Eng.* **8**, 066017 (2011).

91. Ranck, J. B. Which elements are excited in electrical stimulation of mammalian central nervous system: A review. *Brain Res.* **98**, 417–440 (1975).

92. Latikka, J. A., Hyttinen, J. A., Kuurne, T. A., Eskola, H. J. & Malmivuo, J. A. The conductivity of brain tissues: Comparison of results in vivo and in vitro measurements. *Annu. Reports Res. React. Institute, Kyoto Univ.* **1**, 910–912 (2001).

93. Opitz, A., Falchier, A., Linn, G. S., Milham, M. P. & Schroeder, C. E. Limitations of ex vivo measurements for in vivo neuroscience. *Proc. Natl. Acad. Sci.* **114**, 201617024 (2017).

94. Geisler, C. D. & Goldberg, J. M. A Stochastic Model of the Repetitive Activity of Neurons. *Biophys. J.* **6**, 53–69 (1966).

95. Rubinstein, J. T. Analytical theory for extracellular electrical stimulation of nerve with focal electrodes. II. Passive myelinated axon. *Biophys. J.* **60**, 538–555 (1991).

96. Priori, A. Brain polarization in humans: a reappraisal of an old tool for prolonged non-invasive modulation of brain excitability. *Clin. Neurophysiol.* **114**, 589–95 (2003).

97. Esmaeilpour, Z. *et al.* Incomplete evidence that increasing current intensity of tDCS boosts outcomes. *Brain Stimul.* **11**, 310–321 (2018).

98. Datta, A., Truong, D., Minhas, P., Parra, L. C. & Bikson, M. Inter-individual variation during transcranial direct current stimulation and normalization of dose using MRI-derived computational models. *Front. Psychiatry* **3**, 1–8 (2012).

99. Akhtari, M. *et al.* Conductivities of three-layer live human skull. *Brain Topogr.* **14**, 151–67 (2002).

100. Horvath, J. C., Forte, J. D. & Carter, O. Evidence that transcranial direct current stimulation (tDCS) generates little-to-no reliable neurophysiologic effect beyond MEP amplitude modulation in healthy human subjects: A systematic review. *Neuropsychologia* **66**, 213–236 (2015).

101. Wendel, K. & Malmivuo, J. Correlation between Live and Post Mortem Skull

Conductivity Measurements. in *2006 International Conference of the IEEE Engineering in Medicine and Biology Society* **1**, 4285–4288 (IEEE, 2006).

102. Cantürk, İ. *et al.* An experimental evaluation of electrical skin conductivity changes in postmortem interval and its assessment for time of death estimation. *Comput. Biol. Med.* **69**, 92–96 (2016).

103. Krause, M. R. *et al.* Transcranial Direct Current Stimulation Facilitates Associative Learning and Alters Functional Connectivity in the Primate Brain. *Curr. Biol.* **27**, 3086-3096.e3 (2017).

104. Nitsche, M. A. & Bikson, M. Extending the parameter range for tDCS: Safety and tolerability of 4 mA stimulation. *Brain Stimul.* **10**, 541–542 (2017).

105. Tyler, W. J. *et al.* Transdermal neuromodulation of noradrenergic activity suppresses psychophysiological and biochemical stress responses in humans. *Sci. Rep.* **5**, 13865 (2015).

106. Monai, H. *et al.* Calcium imaging reveals glial involvement in transcranial direct current stimulation-induced plasticity in mouse brain. *Nat. Commun.* **7**, 11100 (2016).

107. Ruohonen, J. & Karhu, J. tDCS possibly stimulates glial cells. *Clin. Neurophysiol.* **123**, 2006–2009 (2012).

108. Schwiedrzik, C. M. Retina or visual cortex? The site of phosphene induction by transcranial alternating current stimulation. *Front. Integr. Neurosci.* **3**, 6 (2009).

109. Tyler, W. J. *et al.* Transdermal neuromodulation of noradrenergic activity suppresses psychophysiological and biochemical stress responses in humans. *Sci. Rep.* **5**, 13865 (2015).

110. Heller, L. & van Hulsteyn, D. B. Brain stimulation using electromagnetic sources: theoretical aspects. *Biophys. J.* **63**, 129–38 (1992).

111. Huang, Y. & Parra, L. C. Can transcranial electric stimulation with multiple electrodes reach deep targets? *Brain Stimul.* **12**, 30–40 (2019).

112. Margrie, T., Brecht, M. & Sakmann, B. In vivo, low-resistance, whole-cell recordings from neurons in the anaesthetized and awake mammalian brain. *Eur. J. Physiol.* **444**, 491–498 (2002).

113. Tort, A. B. L., Komorowski, R., Eichenbaum, H. & Kopell, N. Measuring Phase-Amplitude Coupling Between Neuronal Oscillations of Different Frequencies. *J. Neurophysiol.* **104**, 1195–1210 (2010).

114. Schomburg, E. W. *et al.* Theta Phase Segregation of Input-Specific Gamma Patterns in Entorhinal-Hippocampal Networks. *Neuron* **84**, 470–485 (2014).

115. Kadir, S. N., Goodman, D. F. M. & Harris, K. D. High-dimensional cluster analysis with the masked EM algorithm. *Neural Comput.* **26**, 2379–94 (2014).

116. Rossant, C. *et al.* Spike sorting for large, dense electrode arrays. *Nat. Neurosci.* **19**, 634–641 (2016).